

A Climatology of Midlatitude Continental Clouds from the ARM SGP Central Facility:

Part II: Cloud Fraction and Radiative Forcing

Xiquan Dong and Baike Xi

Department of Atmospheric Sciences, University of North Dakota, Grand Forks, ND

Patrick Minnis

NASA Langley Research Center, Hampton, VA

*Corresponding author address:* Dr. Xiquan Dong, The Department of Atmospheric Sciences, University of North Dakota, 4149 Campus Road, Box 9006, Grand Forks, ND58202-9006. Email: [dong@aero.und.edu](mailto:dong@aero.und.edu). Phone: 701-777-6991.

## Abstract

Data collected at the Department of Energy Atmospheric Radiation Measurement (ARM) Southern Great Plains (SGP) central facility are analyzed for determining the variability of cloud fraction and radiative forcing at several temporal scales between January 1997 and December 2002. Cloud fractions are estimated for total cloud cover and for single-layer low (0-3 km), middle (3-6 km), and high clouds (>6 km) using ARM SGP ground-based paired lidar-radar measurements. Shortwave (SW), longwave (LW), and net cloud radiative forcings (CRF) are derived from up- and down-looking standard precision spectral pyranometers and precision infrared radiometer measurements. The annual averages of total, and single-layer, non-overlapped low, middle and high cloud fractions are 0.49, 0.11, 0.03, and 0.17, respectively. Total and low cloud amounts were greatest from December through March and least during July and August. The monthly variation of high cloud amount is relatively small with a broad maximum from May to August. During winter, total cloud cover varies diurnally with a small amplitude, mid-morning maximum and early evening minimum, and during summer it changes by more than 0.14 over the daily cycle with a pronounced early evening minimum. The diurnal variations of mean single-layer cloud cover change with season and cloud height. Annual averages of all-sky, total, and single-layer high, middle, and low LW CRFs are 21.4, 40.2, 16.7, 27.2, and 55.0  $\text{Wm}^{-2}$ , respectively; and their SW CRFs are -41.5, -77.2, -37.0, -47.0, and -90.5  $\text{Wm}^{-2}$ . Their net CRFs range from -20 to -37  $\text{Wm}^{-2}$ . For all-sky, total, and low clouds, the maximum negative net CRFs of -40.1, -70, and -69.5  $\text{Wm}^{-2}$ , occur during April; while the respective minimum values of -3.9, -5.7, and -4.6  $\text{Wm}^{-2}$ , are found during December. July is the month having maximum negative net CRF of -46.2  $\text{Wm}^{-2}$  for middle clouds, and May has the maximum value of -45.9  $\text{Wm}^{-2}$  for high clouds. An uncertainty analysis demonstrates that the

calculated CRFs are not significantly affected by the difference between clear-sky and cloudy conditions. A more comprehensive cloud fraction study from both surface and satellite observations will follow.

## 1. Introduction

Clouds have been classified as the highest priority by the U.S. Climate Change Research Initiative (USCCRI, 2001) because they are one of the largest sources of uncertainty in predicting any potential future climate change (Wielicki et al. 1995; Houghton et al. 2001). Clouds are also the dominant modulators of radiation both at the surface and top of the atmosphere (TOA), and their impact on the Earth's radiation budget mainly depends on bulk properties such as cloud amount, height, and microphysical/optical features (Wielicki et al. 1998; Curry et al. 2000; Houghton et al. 2001). Characterizing cloud radiative effects on the surface is a critical component for understanding the current climate and an important step towards simulating potential climate change. Cloud radiative forcing (CRF) is a simple but effective means of studying cloud-radiation interactions and diagnosing problems in general circulation models (GCM) because the CRF represents the bulk effects of clouds on the surface radiation budget. For instance, the original strong positive cloud feedback in some GCMs decreased (Cess et al. 1990) after the cloud optical properties were changed (Cess et al. 1996).

In last few decades, our knowledge of the radiation budget at the TOA has been improved substantially with the advent of satellite observations from the early Earth Radiation Budget Experiment (ERBE; see Barkstrom, 1984) to the recent Clouds and the Earth's Radiant Energy System (CERES; see Wielicki et al., 1998). Satellite-derived CRFs at the TOA, reported as all-sky CRFs (i.e., the difference between radiative fluxes for clear scenes and for all scenes including clear and cloudy conditions), yield a global net cooling of about  $-17 \text{ Wm}^{-2}$  for the Earth-atmosphere system with the strongest cooling effect occurring in the middle latitudes (Ramanathan et al. 1989). Furthermore, low-level stratiform clouds were identified to have a

strong net cooling effect while thin cirrus clouds appear to have a net warming impact on the Earth-atmosphere system.

Less progress, however, has been made in the development of global climatologies of the radiation budgets in the atmosphere and at the surface due to limited long-term ground-based measurements. To mitigate the impact of the relatively sparse surface network, considerable effort has been focused on estimating the surface radiation budget (SRB) using satellite data. The Global Energy and Water Cycle Experiment (GEWEX) SRB project was established in the late 1980s to retrieve SRB at all locations using operational satellite measurements. Several research groups have estimated surface radiative fluxes based on a variety of empirical parameterizations derived from radiative transfer model calculations, surface measurements, and satellite observations. These parameterizations have used ERBE (Li and Leighton 1993; Tian and Ramanathan 2002) broadband radiation data, cloud data from the International Satellite Cloud Climatology Project (ISCCP) (Zhang et al. 1995; Rossow and Zhang 1995), narrowband spectral radiances from the Geostationary Operational Environmental Satellite (GOES; see Gautier and Landsfeld, 1997), and combinations of CERES cloud data and broadband fluxes (e.g., Charlock et al., 2003; Gupta et al., 2004). The comparisons of the derived surface radiation fluxes with the available surface measurements are generally in good agreement but some of the differences can be as large as  $50 \text{ Wm}^{-2}$  (e.g., Li and Leighton 1993).

In a series of papers, we are developing a climatology of midlatitude continental cloud properties and their impact on the surface radiation budget using data collected at the Department of Energy Atmospheric Radiation Measurement (ARM) Southern Great Plains (SGP) central facility (SCF;  $36.6^\circ\text{N}$ ,  $97.5^\circ\text{W}$ ; see Ackerman and Stokes 2003) from January 1997 to December 2002. In Part I (Dong et al. 2004), we generated a record of single-layer and overcast low-level

stratus cloud macrophysical, microphysical, and radiative properties, and developed a new conceptual model of midlatitude continental low clouds. Here in Part II, we calculate the cloud fractions of total, and single-layer low, middle, and high clouds, and their corresponding CRFs. In this study, we rely entirely on both radar and lidar/ceilometer measurements to identify clear sky, total cloud cover, and single-layer low, middle, and high clouds first, then average clear-sky net (down-up) SW and LW fluxes during a certain time period (a month or season), and finally, calculate the seasonal and monthly mean SW, LW, and net CRF for each category. The present work, with the first long-term complete ground-based observations, should provide more reliable estimates of seasonal, monthly, and hourly variations of cloud fractions and CRFs for climate models to test cloud-radiation-climate interactions. These results should also serve as ground truth for validating climate or single column model simulations over the SGP site.

## **2. Data and analysis methods**

The datasets (5-min resolution) in this study are collected directly or derived from surface measurements. The centerpiece of the cloud instrument array is the millimeter wavelength cloud radar (MMCR; Moran et al., 1998). The MMCR operates at a wavelength of 8 mm in a vertically pointing mode and provides continuous profiles of radar reflectivity from hydrometeors moving through the radar field of view, allowing the identification of clear and cloudy conditions. Cloud-top height ( $Z_{top}$ ) is derived from MMCR reflectivity profiles with the uncertainty of 45 m. Cloud-base height ( $Z_{base}$ ) is derived from a composite of Belfort laser ceilometer, Micropluse Lidar (MPL), and MMCR data (CloudBaseBestEstimate, Clothiaux et al. 2000). Since the laser ceilometer and lidar are sensitive to the second moment of the particle distribution (or the cross-sectional area of the particle) instead of 6<sup>th</sup> moment like the MMCR, the ceilometer and lidar can

provide a more faithful estimate of cloud-base height than MMCR because MMCR often detects precipitation-sized particles below cloud base and a false cloud base due to seasonal insect interference in the MMCR observations at the SCF. The ceilometer and lidar signals, however, can be severely attenuated due to absorption by optically thick liquid cloud layers. These signals can only penetrate through about the lowest 200 m of the cloud (Sassen 1991). Therefore, the ceilometer/lidar derived cloud base height can only be used as the lowest cloud-base height.

The SCF up- and down-looking standard Eppley Precision Spectral Pyranometers (PSPs) and Precision Infrared Pyrgeometers (PIRs) provide measurements of downwelling and upwelling broadband shortwave (SW, 0.3 to 3  $\mu\text{m}$ ) and longwave (LW, 4-50  $\mu\text{m}$ ) fluxes at the surface, respectively. The SW and LW fluxes used in this study are the Best Estimate Flux Value Added Product (VAP) (sgpbeflux1longC1.c1.YYYYMMMDD.hhmmss.cdf, Shi and Long 2002). These VAPs are available starting at March 22, 1997 when three different SCF radiometer systems, SIRS E13, C1, and BSRN/BRS (Baseline Surface Radiation Network, changed to Broadband Radiometer Station in 2001) were in service. An operational algorithm was developed to process data from the three platforms and determine the best flux measurements as VAPs. Prior to that time, the corrected diffuse SW from DiffCorr1Dutt VAP was used as a substitute for the Best Estimate SW Flux VAP. The ideal accuracies of SW and LW fluxes, introduced by Ohmura et al. (1998), are obtained under the “ideal” conditions of cloudless skies and low winds. The best values reported in Table 4 of Shi and Long (2002) represent operational agreement from the three sets of instruments deployed over the long term at the SCF under all-sky and all ambient conditions. Therefore, the real accuracies of downwelling and upwelling SW and LW fluxes in the ARM archived data should be the combination of accuracies from both

Ohmura et al. (1998) and Shi and Long (2002). Those accuracies, listed in Table 1, are  $\sim 10 \text{ Wm}^{-2}$  for the Best Estimate Flux VAP data used in this study.

The cloud fraction  $C$  derived from the paired upward-looking narrow field-of-view radar/lidar measurements is simply the percentage of returns that are cloudy within a specified sampling time period (a month or season), i.e., the ratio of the number of hours when both radar and lidar/ceilometer detected clouds to the total number of hours (all-sky samples) when all measurements were available (lidar/ceilometer and radar measurements, downwelling and upwelling SW and LW fluxes). The total cloud fraction  $C_T$  is the fraction of time that a cloud is detected anywhere in the vertical column, the low cloud fraction  $C_L$  is the fraction of time low clouds ( $Z_{top} < 3 \text{ km}$ ) occur without higher clouds above them, the high cloud amount  $C_H$  is determined for clouds having  $Z_{base}$  higher than 6 km with no lower clouds underneath, while middle clouds ( $C_M$ ) range from 3 to 6 km without any lower and higher clouds below and above (Hartmann et al. 1992). Although  $C_T$ ,  $C_L$ ,  $C_M$ , and  $C_H$  are computed using the same denominator (all-sky samples),  $C_T$  does not equal the sum of  $C_L$ ,  $C_M$ , and  $C_H$  because  $C_T$  includes all cloudy conditions, such as some deep cumulus clouds and multilayered clouds that did not satisfy our definitions of single low/middle/high cloud layers. These cloud fractions should not be confused with an instantaneous hemispheric cloud fraction observed by satellite observations and surface observers. Cloud fraction for the surface observer is the percentage of the sky dome covered by clouds, while for the satellite imager, it is the ratio of the number of pixels within some defined earth surface area.

The change in the net (downwelling minus upwelling) surface radiation balance due to clouds is termed cloud radiative forcing (CRF). It is classified into shortwave ( $CRF_{SW}$ ) and longwave ( $CRF_{LW}$ ) CRF and defined as

$$CRF_{SW} = Q_1 - Q_0 \quad (1a)$$

and

$$CRF_{LW} = F_1 - F_0, \quad (1b)$$

respectively (Ramanathan et al. 1989; Dong and Mace 2003). The CRF is the difference between the net fluxes when clouds are present ( $Q_1$  and  $F_1$ ) and when they are absent ( $Q_0$  and  $F_0$ ,  $C_T = 0$ ), and  $Q$  and  $F$  are the net (downward minus upward) SW and LW fluxes. The NET CRF,  $CRF_{NET}$ , is the sum of  $CRF_{SW}$  and  $CRF_{LW}$  at the surface. All-sky CRF refers to the difference between fluxes averaged for all conditions and for clear skies only. Positive values of CRF indicate surface warming and negative values denote cooling of the surface. Since cloud-base temperature is typically greater than the clear-sky atmospheric effective temperature,  $CRF_{LW}$  is generally positive. The magnitude of  $CRF_{LW}$  is strongly dependent on cloud-base height (i.e., cloud-base temperature) and emissivity. Conversely, clouds reflect more SW flux than clear sky, therefore,  $CRF_{SW}$  is always negative over long time averages or large spatial domains. The magnitude of  $CRF_{SW}$  cooling strongly depends on the cloud optical properties and fraction, and varies with season. In this study, we first calculate monthly and seasonal means of clear-sky SW and LW fluxes, and then compute monthly and seasonal mean net SW and LW fluxes for all sky, total, low, middle, and high clouds. Finally, we determine the corresponding CRFs using (1).

To minimize the impact of different fields of view from the radar/lidar/ceilometer (point of view) and PSP (global, hemispheric) instruments on the clear-sky fluxes, clear-sky periods were identified by radar-lidar data first, and then screened by the ratio of the PSP-measured downwelling SW flux to the inferred clear-sky downwelling SW flux that would be recorded by

PSP if no clouds were present (Long and Ackerman 2000). To avoid the sampling biases in calculating CRF, the SW and LW fluxes under different sky conditions were binned and averaged in 1-hour intervals. The seasonal mean is the average of the 24-hour means within a 3-month period. The monthly mean is the average of the 24-hour means for a given month during the 6-yr period, irrespective of year. Since the CRF is mainly calculated from the difference in net fluxes between cloudy and clear skies, any biases in the flux measurements will tend to cancel out except when the clear-sky and cloudy biases are different. Even so, the difference between downwelling and upwelling fluxes during clear-sky (and cloudy) conditions will also reduce the influence of these biases on the CRF, if both the upward and downward-looking PSPs and PIRs have the same calibrations. To compute 24-hour averages, the SW fluxes are set equal to zero during the night. The four seasons are defined here as winter from December to February (DJF), spring from March to May (MAM), summer from June to August (JJA), and autumn from September to November (SON).

There are a total of ~42,214 hours (~4.82 years) of all-sky samples with nearly equal clear-sky and cloudy occurrences during the 6-yr study period from January 1997 to December 2002 at the ARM SGP central facility (SCF). Note that there are several ways to calculate the monthly and seasonal means from multi-year datasets. Thus, the averages from different methods can be significantly different. Similarly, there are many different ways to define cloud fraction, especially for cloud layers. In this study, the isolated single-layered cloud definitions for  $C_L$ ,  $C_M$ , and  $C_H$  are unique. They provide the basis for independently evaluating the impact of different clouds on the surface radiative budget. In most previous studies, the cloud layers are defined to include those occurring in single and multiple layers or as seen from a satellite. Thus, the

fractional coverage of middle and high-level clouds in this study will be less than that typically reported elsewhere.

### **3. Cloud fraction**

#### *a. Seasonal and monthly variations*

The seasonal variations of total, low, middle, and high cloud fraction from January 1997 to December 2002 are shown in Fig. 1 and summarized in Table 2. Both  $C_T$  (Fig. 1a) and  $C_L$  (Fig. 1b) follow basically the same seasonal patterns with maxima during winter and minima during summer. Single-layer midlevel clouds (Fig. 1c) are the least common and show some tendency for bottoming out during the summer. High cloud fraction (Fig. 1d) tends to be greater during summer than in other seasons. Total annual mean cloud amount varied by 0.112 during the 6 years, from 0.437 (2002) up to 0.549 (1997).

The monthly variations of  $C_T$ ,  $C_L$ ,  $C_M$ , and  $C_H$  during the 6-yr period are illustrated in Fig. 2 and reflect the seasonal patterns seen in Fig. 1. The monthly means of  $C_T$  and  $C_L$  decrease from January to July with the exception of a relative maximum during June, then gradually increase from July to January. The minima in  $C_T$ ,  $C_L$ , and  $C_M$  are found around July and August, while the maxima in  $C_T$  and  $C_L$  occurred from December through March. The monthly variation of  $C_H$  mirrors that of  $C_L$  with local maxima from May through August followed by a significant drop into September that coincides with a rise in  $C_L$ .

#### *b. Diurnal variability*

The hourly means of  $C_T$ ,  $C_L$ ,  $C_M$ , and  $C_H$  were averaged from all their corresponding samples at each local hour from the 6-yr dataset to study the diurnal cycles of different cloud

types over the SCF. The hourly mean cloud fractions are plotted in Fig. 3 where the annual average is calculated from all of the cloud samples and the winter and summer means are calculated from their respective datasets. As demonstrated in Figs. 3a and 3b, the variability in  $C_T$  is primarily driven by  $C_L$ , although the mean value of  $C_L$  accounts for only a fifth of  $C_T$ . The annual and summer hourly means in  $C_T$  and  $C_L$  increase monotonically from midnight (0000 local time - LT) to local noon (1230 LT), then gradually diminish until 1930 LT when they level off for the remainder of the night. During winter, the peaks in  $C_T$  and  $C_L$  occur at ~0930 LT with minima at ~1730 LT. Although the amplitudes  $[(\text{Max}-\text{Min})/2]$  of 0.035 and 0.053 in the annual and winter diurnal cycles in  $C_T$ , respectively, are nearly the same as those for  $C_L$ , 0.032 and 0.066, respectively, the relative variations (to their respective means) in  $C_L$  are about four times larger. The mean diurnal amplitudes in  $C_T$  and  $C_L$  during summer are 0.077 and 0.039 with large relative variations of 19.3% and 78%, respectively. The annual average diurnal cycles include all 4 seasons, but those for  $C_T$  and  $C_L$  in Figs. 3a and 3b appear to be blends of the winter and summer diurnal cycles. Both the winter and summer minima in  $C_L$  occur shortly before sunset, but the lack of an increase in  $C_L$  during the summer night results in the annual minimum occurring at 2100 LT.

The annual and winter diurnal cycles of  $C_H$  are nearly identical: they increase slowly from 0300 LT to 1930 LT, then decrease to 0300 LT during the following day. The two curves diverge for a few hours after 2000 LT when one of the two summer peaks occurs. During summer, the diurnal cycle in  $C_H$  is nearly the opposite of its winter counterpart with maxima in the late evening and around sunrise. During summer, the formation of high cloud cover is often driven by convection whereas during winter, large baroclinic systems cause most of the high clouds. The mean daily amplitudes of annual, winter, and summer  $C_H$  are 0.018, 0.024, and

0.035, respectively, values smaller than those for  $C_T$  and  $C_L$ . Their relative variations are 10.6%, 7.1%, and 16.7%, respectively, comparable to those of  $C_T$  and much smaller than those of  $C_L$ . A local minimum in the  $C_M$  annual mean occurs around 1130 LT with a broad maximum between midnight and sunrise. During summer  $C_M$  has large fluctuations with an early morning minimum and three relative maxima thereafter. All  $C_M$  amplitudes are small (0.01-0.013), but their relative variations are large (33-55%).

### *c. Discussion*

It is noted that the seasonal and monthly means and the diurnal cycle of  $C_L$  in Part I (Dong et al., 2004) are close to, but slightly different from those in this study. In Part I, low cloud was defined as a single-layer and overcast cloud with a cloud-base height less than 3 km and cloud-top height below 4 km, and the cloud lasted up to 2 hours or more to facilitate accurate cloud microphysical and optical property retrievals. The cloud fraction was also simply the percentage of returns that are cloudy within a specified sampling time period, i.e., the ratio of the number of hours when they satisfied the five retrieval criteria to the total number of hours when all instruments (radar, lidar, microwave radiometer, and upward PSP) were working simultaneously. The seasonal and monthly means in  $C_L$  for Part I were divided into day and night. During the 6-yr period, a total of 4002 hours of single-layer and overcast low clouds satisfied the five retrieval criteria and 27,932 hours (~3.2 years) of all-sky samples were taken when all instruments were working simultaneously. The all-sky sampling differences between this study (~4.82 years) and Part I (~3.2 years) are mainly due to the requirement for microwave radiometer measurements in the latter.

The monthly mean values of  $C_T$  (Fig. 2) are plotted in Fig. 4 again for comparison with averages from surface observations reported by Warren et al. (1986) and Lazarus et al. (2000), and from analyses of imagery from the eight Geostationary Operational environmental Satellite (GOES-8) over the SCF (Khayer et al., 2002) updated to include 1997-2002. The seasonal and annual means of  $C_T$ ,  $C_L$ ,  $C_M$ , and  $C_H$  are listed in Table 2. The monthly means of  $C_T$  derived from Warren et al. (1986) were averaged from 11 years of surface observations taken between January 1971 and December 1981 within a  $5^\circ$  region centered near the SCF. Lazarus et al. (2000) averaged surface observations taken during a 10-yr period from December 1981 to November 1991 at two stations, Oklahoma City, OK and Wichita, KS, near the SCF. The GOES-8 results were derived from half-hourly, 4-km radiances taken by GOES-8 daytime observations using the layer bispectral threshold method (LBTM; see Minnis et al. 1995) over an area of  $0.3^\circ \times 0.3^\circ$  centered on the SCF using the same time period as this study. As shown in Fig. 4 and summarized in Table 2, the monthly means of  $C_T$  from four studies agree very well in general trend and magnitude with almost identical annual averages. Similar results were found by Lazarus et al. (2000) using 8 years (1983-1991) of C2 data from the International Satellite Cloud Climatology Project (ISCCP). Although the monthly means from the various datasets are not exactly the same, they all show that cloud cover was greatest during winter and spring, least during summer and fall, and dropped significantly from June to July. Based on this comprehensive comparison (different datasets, spatial scales, and time periods), it is concluded that results presented here for 1997-2002 are typical of the annual  $C_T$  cycle over the SCF.

The seasonal and annual means of  $C_T$ ,  $C_L$ ,  $C_M$ , and  $C_H$  from this study, Warren et al. (1986) and Lazarus et al. (2000) are listed in Table 2. Averaging the ARM SCF data from Fig. 1 yields a winter maximum in  $C_T$  whereas the surface observer averages produce a spring

cloudiness maximum. The GOES-8 seasonal  $C_T$  means (not shown) indicate a spring peak of 53%, but it exceeds the winter average by only 0.6%. Mean total cloud cover from GOES-8 bottoms at 43% during autumn while the other datasets have a summer minimum. Aside from these differences, the seasonal patterns in  $C_T$  are fairly similar with a maximum range of 8% (winter) in the seasonal means for all four datasets.

The  $C_L$ ,  $C_M$ , and  $C_H$  means in Table 2 from the surface observations are much larger than those in this study. This discrepancy is mainly due to the differences in the definitions of low, middle, and high clouds between this study and those two. In this study, the ranges of low, middle, and high clouds are from 0-3 km, 3-6 km, and >6 km without overlap. However, the low, middle, and high clouds from the surface observations include all clouds that occurred in the sky no matter if they occurred in one or multiple layers. The amounts for each layer were also adjusted for random overlap so that the middle and low cloud amounts are larger than what was actually observed. As listed in Table 2, the sum of  $C_L$ ,  $C_M$ , and  $C_H$  is only 63% of  $C_T$  in this study, but it is 122% and 126% in the Warren et al. (1986) and Lazarus et al. (2000) averages, respectively, because they allow up to three layers of clouds in the atmospheric column at any given instant. The GOES-8 layer cloud amounts are not included in Table 2 because of differences in the definitions of low and midlevel clouds. However, the satellite retrieval produced an average fractional coverage of 0.21 for clouds with tops higher than 6 km. This value is between the random-overlap-corrected surface observations and the radar-lidar results and suggests that the random overlap correction may be too extreme.

To further study the occurrence of multilayer clouds at the SCF, Fig. 5 shows the 1-km vertical frequency distribution of cloud occurrence regardless of overlap. The vertical distribution is the ratio of cloud occurrence within a given 1-km interval relative to the total

column cloud occurrence (49% of all samples) during the 6-yr time period. The low, middle, and high cloud frequencies in Fig. 5 are 0.263, 0.231, and 0.506 (the sum of them is 1), those can be converted to 0.13, 0.11, and 0.25 after multiplying by 0.49 (total CF) for comparing to the values in Table 2. From this comparison, we can draw another conclusion, that multilayer clouds are common at the SCF. The motivation for computing one-layer low, middle, and high cloud fractions here is for studying the impact of these cloud layers on the surface radiation budget. A more comprehensive cloud fraction study, including multilayered and overlapped clouds and comparison with GOES results, will be presented in the Part III of this series of papers.

#### **4. Cloud radiation forcing (CRF)**

##### *a. Seasonal and monthly variations of CRFs*

The seasonal mean clear-sky net SW/LW/NET fluxes are shown in Fig. 6a, while all-sky, total, low, middle, and high cloud radiative forcings are shown in Figs. 6b-f. The results are summarized in Table 3. The clear-sky net LW flux is nearly invariant compared to its SW counterpart, ranging from  $-90.8 \text{ Wm}^{-2}$  in spring to  $-74.1 \text{ Wm}^{-2}$  during summer with an annual average of  $-83.1 \text{ Wm}^{-2}$ . The negative net LW flux is mainly due to more LW emission from the surface than from the atmosphere because the surface temperature is much higher than the effective atmospheric radiating temperature during the clear-sky conditions. The maximum and minimum negative net LW fluxes suggest that the temperature differences between the surface and atmosphere are the largest during spring and the least during summer. Details of the seasonal variation can be explored further using the monthly means plotted in Fig. 7a. Since cloudy downwelling LW fluxes are normally greater than those for clear skies, while the upwelling LW fluxes during clear-sky and cloudy conditions are nearly identical, the clear-sky net LW flux is

the largest negative value or more negative than the cloudy net LW flux. Therefore, LW CRFs should be always positive (warming effect on the surface).

The seasonal variation of the clear-sky SW net flux basically follows the seasonal cycles of solar insolation with maxima in summers and minima in winters. The interannual variability for each of the four seasons during the 6-yr period is relatively small ( $\sim 5 \text{ Wm}^{-2}$ ). Monthly mean clear-sky net SW fluxes (Fig. 7a) range from  $104.8 \text{ Wm}^{-2}$  in December to  $276.8 \text{ Wm}^{-2}$  in June, which correspond to the winter and summer solstices, respectively. Since clouds can partially block the incident solar insolation to the surface, the clear-sky net SW flux is the maximum amount of solar radiation absorbed by the surface except for broken cumulus cases. Therefore, SW CRFs should be always negative (cooling effect on the surface) over long time averages or large spatial domains. Since the clear-sky net LW flux is relatively constant throughout the year and small in magnitude compared to the SW flux, the seasonal and monthly variations of total (or NET) flux are primarily determined by net SW flux with maxima in summers and minima in winters.

As demonstrated in Figs. 6 and 7, the seasonal and monthly variations of LW and SW CRFs for all-sky, total, and low clouds are very similar to each other with increasing amplitudes from all-sky, total to low clouds where the magnitudes and variations of their LW CRFs are much smaller than their SW counterparts. As seen in Table 3, the minimum LW CRFs occur during summer (Figs. 6b-6d), specifically during the July-August period in the monthly means (Figs. 7b-d). The corresponding seasonal mean SW CRFs decrease significantly from the winter maxima to the spring minima (the maximum negative values). More precisely, the monthly means are most negative during April and least negative during the November-February period. Consequently, the net CRFs are primarily determined by the SW CRFs. Thus, the largest negative

net CRFs occur during spring and the smallest negative values occur during winter. April is the month having the greatest negative forcing. During winter, the negative SW CRFs and positive LW CRFs nearly cancel each other resulting in NET CRFs between 0 and  $-10 \text{ Wm}^{-2}$ . Although the magnitudes of both SW and LW CRFs for total cloud cover are smaller than those for low clouds, the total cloud NET CRFs during the four seasons are comparable to, or even slightly larger than, those for low clouds.

The seasonal and monthly variations of LW/SW/NET CRFs for high clouds (Fig. 6f) nearly mimic the CRFs of all sky. The maximum negative SW and NET CRFs occur seasonally during spring and summer, and monthly during the May-June period. The magnitude is smallest during winter. The high-cloud LW CRFs are nearly invariant with season. The magnitudes of LW/SW/NET CRFs for the middle clouds (Fig. 6e) are slightly larger than those for high clouds with the maximum positive LW CRFs during fall and the maximum negative SW CRFs during summer. Midlevel cloud NET CRFs basically follow the SW CRF variations, but they are sometimes slightly positive when the LW warming effect overwhelms the SW cooling effect during winter. September has the largest positive LW forcing, and July has the maximum negative SW and NET CRFs.

### *b. Diurnal variability*

The hourly mean clear-sky net LW/SW/NET fluxes and CRFs from the 6-yr dataset are plotted in Fig. 8. As expected, the intensity of solar insolation (Fig. 8a) follows the solar zenith angle. During night, the upwelling LW flux is consistently higher than downwelling LW flux, and its net value is almost constant (negative). The net LW flux decreases rapidly after sunrise reaching the maximum negative value around the local noon ( $\sim 1200\text{-}1400 \text{ LT}$ ) as a result of

surface heating from the insolation. The total or NET radiation is negative at night, being completely determined by net LW flux. A surplus in the NET flux begins right after sunrise following the same pattern as net SW flux. The deficit starts just before sunset when the surface-emitted LW flux exceeds the sum of solar insolation and atmosphere-emitted LW flux.

The hourly mean LW CRFs for all-sky, total, low, middle, and high clouds are plotted in Fig. 8b. The minima occur during night while the largest values are found around the local noon. All LW CRFs during night are nearly constant with a range of  $10 \text{ W m}^{-2}$  (high cloud) to  $40 \text{ W m}^{-2}$  (low cloud), then start to rise monotonically after sunrise until the local noon with a range of  $20 \text{ W m}^{-2}$  (high cloud) to  $80 \text{ W m}^{-2}$  (low cloud), and finally diminish gradually until sunset remaining nearly constant for the rest of the night. The hourly variations of all LW CRFs basically follow their clear-sky LW patterns but in an opposite sign. The hourly variation of middle-cloud LW CRF is slightly irregular, which may be due to limited middle-cloud samples (Fig. 3c). During the calculation of these CRFs, the clear-sky net LW flux is the same and the upwelling (surface temperature) LW fluxes during different sky conditions are also nearly the same. Therefore, these LW CRFs are mainly determined by the downwelling LW fluxes under different sky conditions. The downwelling LW fluxes of clouds are primarily determined by cloud height (temperature) and microphysical properties such as emissivity ( e.g., Shupe and Intrieri 2004). High clouds, with lower cloud-base temperature and emissivity, produce a small downwelling LW radiation, which has been mostly absorbed by the abundance of atmospheric moisture before it arrives the surface. Consequently, the high-cloud-emitted downwelling LW radiation at the surface is small and only slightly larger ( $10\text{-}20 \text{ W m}^{-2}$ ) than clear-sky value. Conversely, the downwelling LW flux from low clouds is significantly higher than from clear-sky and higher clouds due to the warm cloud-base temperature and nearly blackbody emissivity.

Also, the water vapor path length is reduced between the cloud base and the surface allowing more of the low-cloud-emitted downwelling LW radiation to reach the surface.

The hourly variations of SW CRFs for all-sky, total, low, middle, and high clouds mirror the clear-sky SW flux with the maximum negative values around local noon. Downwelling SW radiation at the surface is primarily determined by solar insolation (solar zenith angle) and cloud optical depth, as well as water vapor absorption above and below the cloud layer. Low clouds have the largest negative SW forcing because most of them are optically thick (Dong et al. 2004). The opposite is true for high cloud because most of them are optically thin (Mace et al. 2001; Wang et al. 2002). The SW CRFs for all-sky, total, and middle clouds are similar to their LW counterparts, with values between those of high and low clouds, and the middle-cloud SW CRF behaves like its LW counterpart. The NET CRFs under different sky conditions are mainly determined by their SW CRFs during daytime, and entirely by their LW CRFs during night. Low clouds have the strongest cooling effect during day and the largest warming effect during night, and have an overall strong cooling effect on the surface. High clouds have the least warming effect during night and cooling effect during day comparing to other clouds with an overall weak cooling effect on the surface. The LW/SW/NET CRFs of all sky and middle clouds are similar to those of high clouds, while the total-cloud CRFs are close to low clouds.

The hourly means of winter and summer clear-sky LW/SW/NET fluxes and CRFs are illustrated in Figs. 9a and 9e, respectively, and summarized in Table 3, where the clear-sky net SW flux during winter is much smaller than summer and other seasons due to shorter daytime duration and smaller intensity of solar insolation. However, the clear-sky net LW flux during winter is more negative than during summer, suggesting that the temperature difference between surface and atmosphere during winter is larger than during summer. The ground-based

microwave radiometer derived integrated water vapor during summer ( $\sim 4$  cm) is substantially higher than that during winter ( $\sim 1$  cm) (see Section 4d). Since the downwelling LW flux positively correlates with the integrated water vapor of the atmosphere, there is more LW flux loss at the surface during winter than during summer despite the greater summer surface temperatures.

The diurnal variations of LW CRFs are much stronger during winter than during summer for total and low clouds, and relatively weak for all-sky, middle and high clouds. Further study reveals that the strong diurnal variations of total-cloud and low-cloud LW CRFs are mainly due to the larger downward LW flux difference between cloudy and clear-sky conditions during winter than during summer. The upward LW flux difference between cloudy and clear-sky conditions during winter, however, is close to that during summer. Although the amplitudes of the SW CRFs during winter and summer are comparable, the duration of solar radiation in winter is much shorter, therefore the overall averages of the SW CRFs in winter are much smaller (absolute value) than in summer. The NET CRFs during winter are nearly neutral, or vary around zero because the positive LW forcings cancel out the negative SW forcings. During summer, the NET CRFs are much more negative. The unpredictable middle-cloud SW/LW/NET CRFs in both winter and summer seasons, as well as in annual, indicate that the hourly means of these CRFs may not be reliable due to limited cloud samples. This result further suggests that the study includes a sufficient number of samples to calculate statistically reliable CRFs for all cloud types, except middle clouds.

### *c. Downwelling SW and LW fluxes*

The seasonal, monthly, and hourly means of downwelling SW and LW fluxes are shown in Figs. 10-12, and their seasonal and annual means listed in Table 4. As demonstrated in Figs. 10a and 11a, the seasonal and monthly variations of downwelling SW fluxes have peaks in summers and troughs in winters for both clear-sky and cloudy conditions. These patterns are primarily controlled by changes in the intensity and duration of incoming solar radiation, and partially dependent of cloud optical properties. Clear sky has the maximum solar transmission, low clouds have the minimum, and other clouds are between clear sky and low clouds. However their downwelling LW fluxes are in the reverse order relative to their solar transmissions, where low clouds have the maximum downwelling LW flux and clear sky has the minimum as shown in Figs. 10b and 11b. The monthly variation of downwelling LW fluxes has the same pattern as that of integrated atmospheric water vapor (see Section 4d) with the minimum value in January and the maximum value in July. The hourly means of downwelling SW fluxes for annual, winter and summer seasons are illustrated in Fig. 12 with very similar patterns to their CRF counterparts.

Overall, the seasonal, monthly, and hourly means of downwelling SW and LW fluxes are very similar to their CRF counterparts, and can be summarized as three groups. The group 1 includes only clear sky with the maximum SW flux and the minimum LW flux, and the group 2 includes total and low clouds in opposite direction to the group 1 with the minimum SW flux and the maximum LW flux. The group 3 includes all sky, middle and high clouds, and their SW and LW fluxes are between the group 1 and the group 2.

Figure 13 shows the comparisons between this study and other research groups derived surface SW fluxes from both empirical parameterizations and satellite observations. The monthly downwelling all-sky SW fluxes in this study are used to compare with those in the Gautier and

Landsfeld (1997) study, where they used 14 months of the Geostationary Operational Environmental Satellite (GOES-7) data during March 1993 to April 1994 period over an area of 250-km X 250-km centered on the ARM SCF. The monthly downwelling SW fluxes in this study are systematically higher ( $\sim 30 \text{ Wm}^{-2}$ ) than those in the Gautier and Landsfeld study (Fig. 13a). This discrepancy may be due to (1) different data sets (surface vs. satellite and model), (2) spatial coverages (a point vs. 250-km X 250-km), and (3) time periods (6 years from Jan. 1997 to Dec. 2002 vs. 14 months from March 1993 to April 1994) between these two studies. However, there is an excellent agreement in the monthly clear-sky and all-sky net SW fluxes and CRFs between this study and Li and Leighton (1993) as shown in Figs. 13 b-d. The Li and Leighton (1993) results consist of values derived from 5 years of ERBE data (November 1984 – December 1989) for two  $2.5^\circ \times 2.5^\circ$  boxes between  $35$  and  $37.5^\circ\text{N}$ , and longitudes  $95$  to  $97.5^\circ\text{W}$  (Li\_B) and  $97.5$  to  $100^\circ\text{W}$  (Li\_A). Since the SCF is located on the boundary of the Li and Leighton boxes, it is necessary to compare the SCF results to the averages for both boxes. The annual averages of net clear-sky and all-sky SW fluxes from both studies agree within  $6 \text{ Wm}^{-2}$ . The CRFs in this study are between the values of the two boxes. The small differences between the results suggest that the SCF values are representative of a much larger area.

#### *d. Uncertainties*

The biases in data sampling and processing are one potential problem in calculating CRFs from observational data. To minimize the biases, both clear-sky and cloudy fluxes were binned and averaged in 1-hr intervals, and the seasonal (monthly) means of clear-sky flux and CRF were averaged from 24-hr averaged values in a season (or one of 12 months during the 6-yr period). Thus, the samples in each hour are equally weighted in calculating the seasonal or

monthly mean. Besides the biases, imperfect clear-sky screening is one of the major uncertainties in calculating CRFs because the seasonal and monthly means of clear-sky fluxes can be easily contaminated by a few percent cloud cover, which would artificially increase SW CRFs and decrease LW CRFs. To have the most accurate clear-sky fluxes, we used the ARM radar/lidar/ceilometer observations to identify clear-sky conditions first, then use the ratio ( $>0.7$ ) of PSP-measured downwelling SW flux to the inferred clear-sky flux further screen the data. Different ratio values, such as 0.8 and 0.9, provided almost the same the clear-sky SW and LW fluxes as 0.7 but with fewer clear-sky samples. The annual average net SW flux increases from 191.1 to 196.8  $\text{Wm}^{-2}$ , and the annual average of net LW flux decreases from -80.9 to -83.1  $\text{Wm}^{-2}$  after applying the ratio test, indicating that additional cloud cover was removed from the clear-sky data.

In addition to the biases and clear-sky screening, another important uncertainty source is the clear-sky background information because the clear-sky fluxes are used as references in calculating CRFs. Before we study the impact of this uncertainty on the calculated CRFs, we should answer the following two questions. 1) What are the differences in surface albedo and upwelling LW flux between clear-sky and cloudy conditions? How much are the calculated CRFs affected when we use the clear-sky fluxes as references in this study? 2) What are the differences in atmospheric aerosol and water vapor between clear-sky and cloudy conditions? How much do these differences impact on the calculated CRFs in this study ?

The monthly mean surface albedos (Fig. 14a) during clear-sky periods are normally about 0.01-0.02 higher than those for cloudy periods (except for December). The differences can arise for several reasons including the solar zenith angle (SZA) and surface moisture. In clear skies, the surface albedo varies with SZA as a result of scattering of the direct beam by surface

components. As the cloud cover thickens, the downwelling SW radiation becomes almost totally diffuse so the direct beam scattering is no longer a factor, and its albedo becomes independent of SZA and corresponds to the albedo at an SZA around 55°. Since the albedo is greater at higher values of SZA, the clear-sky albedo represents an integration of the albedos over all SZAs, and the mean  $\cos(\text{SZA})=0.41449$  during the 6-yr clear-sky period at the SCF corresponds to an SZA =65.5°, thus the clear-sky albedo is, on average, larger than the cloudy-sky albedo. Increased soil moisture tends to darken a surface, so that in rainy conditions and after rain, the surface will be darker than average. Except for short-lived thunderstorms, rain is normally accompanied by considerable cloud cover and the cloud cover prevents rapid drying of the surface by decreasing the available SW flux. Thus the soil moisture should, on average, be greater during overcast conditions than under clear skies.

The greater surface albedo during the cloudy period in December is mainly determined by four heavy snow periods that lasted for a few days from the beginning to end. The four snowy time periods are (1) December 13-15, 2000, (2) December 26-30, 2000, (3) December 4-7, 2002, and (4) December 23-29, 2002. There was almost no snow effect on the clear-sky surface albedo in December except for December 16-18, 2000. There was a heavy snow period from December 31, 2000 to January 6, 2001, with cloudy period from December 31, 2000 to January 2, 2001, and clear-sky period for the remaining four days (January 3-6, 2001). The annual difference in surface albedo between clear and cloudy skies is 0.011 (or ~5%), which results in an annual difference of  $-2.7 \text{ Wm}^{-2}$  [ $\text{SW}_{\text{clr}}*(R_{\text{cld}}-R_{\text{clr}})$ ], suggesting the modified SW CRFs would be  $2.7 \text{ Wm}^{-2}$  lower than the current values if the cloudy surface albedo was used to calculate the clear-sky reflected SW flux.

The monthly mean upwelling LW fluxes during both clear and cloudy periods are shown in Fig. 14b with their differences in Fig. 14c. The annual mean upwelling LW fluxes during cloudy periods are  $-5.5 \text{ Wm}^{-2}$  smaller than those in clear skies, mainly as a result of the large difference in summer. The overall effect (NET difference) is  $-8.2 \text{ Wm}^{-2}$ , indicating that the modified NET CRFs would be  $8.2 \text{ Wm}^{-2}$  lower than the current values if we used the cloudy surface albedo and upwelling LW flux as clear-sky references in calculating CRFs.

Li and Trishchenko (2001) argued that aerosol and water vapor are the main factors affecting clear-sky fluxes, and that the water vapor difference between cloudy and clear-sky conditions has a much larger effect on downwelling SW flux than aerosol. Therefore, we focus on determining how much the difference in the microwave radiometer-retrieved precipitable water vapor (PWV) between cloudy and clear-sky periods can affect the CRF calculations. The downwelling SW (LW) flux differences in Plate 1 are calculated from the flux averages in a 1-cm interval of PWV with respect to their monthly SW (LW) means under the clear-sky conditions. The NET flux difference is simply the sum of SW and LW flux differences at each 1-cm interval of PWV. The monthly variation patterns in the SW, LW, and NET flux differences basically follow the monthly variation of PWV (Fig. 16a), and dark green between light green and light blue represents their monthly mean values. It is obvious that the downwelling SW flux at the surface is smaller (greater) when PWV is greater (less) than its monthly mean. The converse is true for LW flux.

To quantitatively study the relationships between clear-sky downwelling SW and LW fluxes with PWV, we plot Fig. 15 where the 1728 (6yr X 12month X 24hr) hourly means of PWV, downwelling  $\text{SW}/\mu_0$ , and LW fluxes are sorted and averaged in a 0.5-cm interval of PWV using the 6-yr clear-sky dataset. The  $\text{SW}/\mu_0$  and LW fluxes are then parameterized as a

logarithmic function of PWV resulting in very high correlations as illustrated in Fig 15a & b. The SW flux is normalized to zenith path with the cosine of solar zenith angle  $\mu_0$ . As demonstrated in Fig. 15a & b, the normalized SW flux decreases and the LW flux increases smoothly with increasing PWV.

Figure 16 is used to help quantify the uncertainties in the downwelling SW and LW fluxes due to different clear-sky and cloudy backgrounds. Figure 16a shows the monthly means of clear-sky and cloudy PWV during the 6-yr period. The annual average clear-sky PWV is about 75% of the cloudy PWV but varies seasonally from 59% in December up to 89% in August. Figures 16b and c present the monthly mean measured clear-sky downwelling SW and LW fluxes (the same values as in Fig. 11a & b) and recalculated values using the new parameterizations (Fig. 15) with the input of the monthly cloudy PWVs in Fig. 16a. The LW parameterization from Fig. 15b is directly applied in the calculation, while the monthly clear-sky solar zenith angle and daytime hours (the ratio of daytime hours to 24 hrs) are used in the SW flux calculation. There are less downwelling SW flux and more LW flux using the cloudy PWV in the new parameterizations relative to their clear-sky measured values. The SW and LW effects are canceled in the overall NET effect as shown in Fig. 16d, but with relatively large fluctuations month by month.

In general, the NET CRFs would be slightly small ( $\sim 8.2 \text{ Wm}^{-2}$ ) if the cloudy surface albedo and upwelling LW flux were used in the calculation of CRF. The annual NET CRFs in this study should not be affected significantly by the differences of clear-sky and cloudy conditions although the SW and LW CRFs may be more or less affected for individual months. The uncertainties in data sampling and clear-sky screening have negligible impact on the CRF calculations.

## 5. Summary and Conclusions

A 6-yr record of total, and one-layer low, middle, and high cloud fractions, and their corresponding cloud radiative forcings have been generated from the ground-based measurements at the ARM SGP central facility during the January 1997-December 2002 period. This record documents the most comprehensive and accurate dataset to date on continental cloud fractions and radiative forcings. It facilitates detailed examination of the seasonal, monthly, and hourly variations of total, low, middle, and high clouds and the impact of these clouds on the surface radiative budget. From the 6-yr results and comparisons with other studies, we have found the following:

- 1) At the SCF, (a) the total and low cloud covers are greatest during winter and spring and least during summer; (b) single-layer high clouds occur more frequently in all four seasons than other types of clouds with a peak in summer; (c) single-layer midlevel clouds occur less frequently than others with a small seasonal variation; and (d) multilayer clouds are common.
- 2) LW and SW CRFs for all-sky conditions and for total and low clouds are very similar to each other with larger seasonal amplitudes than other cloud types. Minimum LW CRF occurs during summer and the maximum negative SW CRF occurs in spring. NET CRF for those cloud types is most negative in spring and least negative during winter. Maximum negative SW and NET CRFs for high clouds occur in spring and summer with the minimum occurring during winters. The LW CRF is nearly invariant seasonally. For middle clouds, September is the month having the largest positive LW forcing, and July has the maximum negative SW and NET forcings.
- (3) Low clouds have the strongest cooling effect during day and the largest warming effect during night with an overall strong cooling effect on the surface. High clouds have the least warming effect during night and cooling effect during day compared to other clouds with an

overall weak cooling effect on the surface. The LW/SW/NET CRFs for all sky conditions and middle clouds are similar to those of high clouds, while those of total clouds are close to low-cloud CRFs.

4) The uncertainties in data sampling and clear-sky screening have essentially no impact on the calculated CRFs in this study. The annual NET CRFs in this study should not be affected significantly by different clear-sky and cloudy backgrounds although the SW and LW CRFs may be more or less affected at individual month. The NET CRFs would average  $\sim 8.2 \text{ Wm}^{-2}$  less if the cloudy surface albedo and upwelling LW flux were used in the calculation of CRF.

The results of the analysis of the 6-yr ARM SCF dataset in this study should provide more reliable estimations of seasonal, monthly, and diurnal variations of cloud fractions and CRFs for climate modelers to test cloud-radiation-climate interactions. These results should serve as baselines for studying radiation budget at the surface, and atmospheric radiation budget when combined with satellite measurements at top of the atmosphere. These results should also serve as the ground truth for validating satellite results and climate or single column model simulations over the SGP site.

***Acknowledgements:*** Data were obtained from the Atmospheric Radiation Measurement (ARM) Program sponsored by the U.S. Department of Energy (DOE) Office of Energy Research, Office of Health and Environmental Research, Environmental Sciences Division. Special thanks to Drs. Thomas P. Ackerman and Charles N. Long at DOE PNNL for providing useful suggestions and comments, to Dr. Zhanqing Li at University of Maryland for providing the surface fluxes derived from ERBE, and to Mandy Khaiyer and Dung Phan for providing the GOES-8 cloud amount averages. This research was supported by NASA CERES project under grant NNL04AA11G at the University of North Dakota. During this study, authors were also supported by DOE ARM program under Interagency Agreement DE-AI02-97ER62341 and University of North Dakota Faculty Seed Funding.

## REFERENCES

- Ackerman, T. P., and G. M. Stokes, 2003: The Atmospheric Radiation Measurement Program. *Physics Today*, **56**, 38-44.
- Barkstrom, B. R., 1984: The Earth Radiation Budget Experiment. *Bull. Amer. Meteor. Soc.*, **65**, 1170-1185.
- Cess, B., and Coauthors, 1990: Intercomparison and interpretation of climate feedback processes in 19 atmospheric general circulation models. *J. Geophys. Res.*, **95**, 16 601-16 615.
- Cess, B., and Coauthors, 1996: Cloud feedback in atmospheric general circulation models: An update. *J. Geophys. Res.*, **101**, 12 791-12 794.
- Charlock, T. P., F. G. Rose, and D. A. Rutan, 2003: Validation of the archived CERES surface and atmospheric radiation budget (SARB). *Proc. 13th ARM Sci. Team Mtg.*, Broomfield, CO, Mar 31 - Apr 4 (Available at [http://www.arm.gov/publications/proceedings/conf13/extended\\_abs/charlock-tp.pdf](http://www.arm.gov/publications/proceedings/conf13/extended_abs/charlock-tp.pdf))
- Clothiaux, E.E., T.P. Ackerman, G.G. Mace, K.P. Moran, R.T. Marchand, M.A. Miller, and B.E. Martner, 2000: Objective determination of cloud heights and radar reflectivities using a combination of active remote sensors at the Atmospheric Radiation Measurement Program Cloud and Radiation Test Bed (ARM CART) sites. *J. Appl. Meteor.*, **39**, 645-665.
- Curry, J.A., and Coauthors, 2000: FIRE Arctic Clouds Experiment. *Bull. Amer. Meteor. Soc.*, **81**, 5-29.
- Dong, X., and G.G. Mace, 2003: Arctic stratus cloud properties and radiative forcing derived from ground-based data collected at Barrow, Alaska. *J. Climate*, **16**, 445-461.

- Dong, X., P. Minnis, and B. Xi, 2004: A climatology of midlatitude continental clouds from the ARM SGP Central Facility: Part I: Low-level cloud macrophysical, microphysical and radiative properties. *J. Climate*. In press.
- Gautier, C., and M. Landsfeld, 1997: Surface solar radiation flux and cloud radiative forcing for the Atmospheric Radiation Measurement (ARM) Southern Great Plains (SGP): A satellite, surface observations, and radiative transfer model study. *J. Atmos. Sci.*, **54**, 1289-1307.
- Gupta, S. K., D. P. Kratz, A. C. Wilber, and L. C. Nguyen, 2004: Validation of the Langley parameterized algorithms used to derive the CERES/TRMM surface radiative fluxes. *J. Atmos. Ocean. Tech.*, **21**, 742-752.
- Hartmann, D.L., M.E. Ockert-Bell, and M.L. Michelsen, 1992: The effect of cloud type on Earth's energy balance: Global analysis. *J. Climate*, **5**, 1281-1304.
- Houghton, J.T., and coauthors, 2001: *Climate Change 2001: The Scientific Basis*. Cambridge University Press.
- Khayer, M. M., A. D. Rapp, P. Minnis, D. R. Doelling, W. L. Smith, Jr., L. Nguyen, M. L. Nordeen, and Q. Min, 2002: Evaluation of a 5-year cloud and radiative property dataset derived from GOES-8 data over the Southern Great Plains. *Proc. 12th ARM Science Team Meeting*, April 8-12, St. Petersburg, FL, (Available at [http://www.arm.gov/docs/documents/technical/conf\\_0204/khayer-mm.pdf](http://www.arm.gov/docs/documents/technical/conf_0204/khayer-mm.pdf))
- Lazarus, S.M., S.K. Krueger, and G.G. Mace, 2000: A cloud climatology of the Southern Great Plains ARM CART. *J. Climate*, **13**, 1762-1775.
- Li, Z., and H.G. Leighton, 1993: Global climatologies of solar radiation budgets at the surface and in the atmosphere from 5 years of ERBA data. *J. Geophys. Res.*, **98**, 4919-4930.

- Li, Z., and A.P. Trishchenko, 2001: Quantifying uncertainties in determining SW cloud radiative forcing and cloud absorption due to variability in atmospheric conditions. *J. Atmos. Sci.*, **58**, 376-389.
- Long, C.N., and T.P. Ackerman, 2000: Identification of clear skies from broadband pyranometer measurements and calculation of downwelling shortwave cloud effects. *J. Geophys. Res.*, **105**, 15 609-15 626.
- Mace, G.G., E.E. Clothiaux, and T.P. Ackerman, 2001: The composite characteristics of cirrus clouds: Bulk properties revealed by one year of continuous cloud radar data. *J. Climate*, **14**, 2185-2203.
- Minnis, P., W.L. Smith, Jr., D.P. Garber, J.K. Ayers, and D.R. Doelling, 1995: Cloud properties derived from GOES-7 for the spring 1994 ARM Intensive Observing Period using version 1.0 of the ARM satellite data analysis program. *NASA RP 1366*, 59 pp.
- Moran, K.P., B.E. Martner, M.J. Post, R.A. Kropfli, D.C. Welsh, and K.B. Widener, 1998: An unattended cloud-profiling radar for use in climate research. *Bull. Amer. Meteor. Soc.*, **79**, 443-455.
- Ohmura, A.E., and Coauthors, 1998: Baseline Surface Radiation Network (BSRN/WCPCP): New precision radiometry for climate research. *Bull. Amer. Meteor. Soc.*, **79**, 2115-2136.
- Ramanathan, V., R.D. Cess, E.F. Harrison, P. Minnis, B.R. Barkstrom, E. Ahmad, and D. Hartmann, 1989: Cloud-radiative forcing and climate: Results from the Earth Radiation Budget Experiment. *Science*, **243**, 57-63.
- Rossow, W.B., and Y.-C. Zhang, 1995: Calculations of surface and top-of-atmosphere radiative fluxes from physical quantities based on ISCCP data sets, 2. Validation and first results. *J. Geophys. Res.*, **100**, 1166-1197.

- Sassen, K., 1991: The polarization lidar technique for cloud research: A review and current assessment. *Bull. Amer. Meteor. Soc.*, **79**, 197-219.
- Shi, Y., and C.N. Long, 2002: Best Estimate Radiation Flux Value-Added Procedure: Algorithm operational details and explanations. DOE ARM Technical report TR-08 [Available online at [http://www.arm.gov/publications/tech\\_reports/arm-tr-008.pdf](http://www.arm.gov/publications/tech_reports/arm-tr-008.pdf)].
- Shupe, M., and J.M. Intrieri, 2004: Cloud radiative forcing of the arctic surface: The influence of cloud properties, surface albedo, and solar zenith angle. *J. Clim.*, **17**, 616-628.
- Tian, B., and V. Ramanathan, 2002: Role of tropical clouds in surface and atmospheric energy budget. *J. Climate*, **15**, 296-305.
- Wang, Z., and K. Sassen, 2002: Cirrus cloud microphysical property retrieval using lidar and radar measurements. Part II: Midlatitude cirrus microphysical and radiative properties. *J. Atmos. Sci.*, **59**, 2291-2302.
- Warren, S.G., C.J. Hahn, J. London, R.M. Chervin, and R.L. Jenne, 1986: Global distribution of total cloud cover and cloud type amounts over land. NCAR Tech. Note, *NCAR/TN-273+STR*, 229 pp., Natl. Cent. for Atmos. Res., Boulder, Colo.
- Wielicki, B.A., R.D. Cess, M.D. King, D.A. Randall, and E.F. Harrison, 1995: Mission to Planet Earth Role of clouds and radiation in climate. *Bull. Amer. Meteor. Soc.*, **76**, 2125-2153.
- Wielicki, B.A., and Coauthors, 1998: Clouds and the Earth's Radiant Energy System (CERES): Algorithm Overview. *IEEE Transaction on Geoscience and Remote Sensing*. **36**, 1127-1141.
- Zhang, Y.-C., W.B. Rossow, and A.A. Lacis, 1995: Calculations of surface and top-of-atmosphere radiative fluxes from physical quantities based on ISCCP data sets, 1. Method and sensitivity to input data uncertainties. *J. Geophys. Res.*, **100**, 1149-1165.

### Figure Captions

Fig. 1. The four seasons used in this study are DJF (winter), MAM (spring), JJA (summer), and SON (autumn). The total, and one-layer low ( $Z_t \leq 3$  km), middle ( $Z_b > 3$  km,  $Z_t \leq 6$  km), and high ( $Z_t > 6$  km) cloud fractions are defined as the lidar-radar measured cloud samples to the all-sky samples when all instruments of lidar/ceilometer, radar, downward and upward PSPs and PIRs were working simultaneously from January 1997 to December 2002 at the ARM SGP central facility (SCF). The dotted lines represent 6 summers during the 6-yr period.

Fig. 2. Same as Figure 1, except for monthly means of cloud fractions derived from the 6-yr ARM SCF dataset.

Fig. 3. Hourly averages of total, one-layer low, middle, and high cloud fractions for annual, winter, and summer seasons from the 6-yr dataset at the ARM SCF.

Fig. 4. The Warren et al. and Lazarus et al. studies were calculated from surface observations from January 1971 to December 1981 in a  $5^\circ$  region centered near the SCF, and from December 1981 to November 1991 at two stations (Oklahoma City, Oklahoma, and Wichita, Kansas) nearby the SCF, respectively. The GOES results are averaged over an area of  $0.3 \times 0.3$  degree centered on the SCF with the same time period as this study.

Fig. 5. Vertical distributions (1-km resolution) of total clouds at the ARM SCF during the 6-yr period.

Fig. 6. Seasonal means of clear-sky net (down-up) LW and SW fluxes are calculated from the upward and downward PIR and PSP measurements when the sky was identified as cloudless by lidar-radar measurements. The seasonal LW (SW) CRF is the difference between cloudy and clear-sky LW (SW) means, and the seasonal net CRF is the sum of LW and SW CRFs (the values of net CRF are negative for cooling and positive for warming of the surface).

Fig. 7. Same as Figure 6, except for monthly means of clear-sky fluxes and cloud radiative forcings calculated from the 6-yr ARM SCF dataset.

Fig. 8. Hourly averages of (a) clear-sky net SW/LW/NET fluxes, (b) LW, (c) SW, and (d) NET CRFs of all sky, total, low, middle, and high clouds during the 6-yr period at the ARM SCF.

Fig. 9. Same as Figure 8, except for winter and summer seasons.

Fig. 10. Seasonal means of downwelling SW and LW fluxes measured by upward PSP and PIR, respectively, at the ARM SCF during the 6-yr period.

Fig. 11. Same as Figure 10, except for monthly means.

Fig. 12. Same as Figure 10, except for hourly means of annual, and winter and summer seasons.

Fig. 13. The overall means are averaged from 12-month means. The monthly means of surface SW fluxes and CRFs in this study represent a point measurements at the SCF (36.6°N, 97.5°W) from January 1997 to December 2002, in Li and Leighton study represent a 2.5° X 2.5° spatial average including latitudes of 35 to 37.5°N, and longitudes of 95 to 97.5°W (Li\_B) and 97.5 to 100°W (Li\_A) from 5 years of ERBE data during the period of November 1984 to December 1989. The Gautier and Landsfeld results were averaged from 14 months of GOES-7 data between March 1993 and April 1994 over an area of 250-km X 250-km centered on the SCF.

Fig. 14. Monthly means of clear-sky and total-cloud surface albedos (a) and upwelling LW fluxes (b). The monthly means of SW flux difference ( $\Delta SW$ ) are the product of downwelling clear-sky SW flux and surface albedo difference between clear sky and cloudy [ $SW_{clr}(R_{cld} - R_{clr})$ ],  $\Delta LW = LW_{cld} - LW_{clr}$ , and  $\Delta NET = \Delta SW + \Delta LW$ .

Fig. 15. Parameterizations of clear-sky downwelling SW/ $\mu_0$  and LW fluxes with precipitable water vapor (PWV) from a 0.5-cm interval (means and standard deviation) during the 6-yr period at the SCF.

Fig. 16. (a) Monthly means of PWV during clear-sky and cloudy conditions, (b) the clear-sky downwelling measured SW/ $\mu_0$  flux and calculated SW/ $\mu_0$  flux using the new parameterization with cloudy PWV, (c) the clear-sky downwelling measured LW flux and calculated LW flux using the new parameterization with cloudy PWV, and (d) the difference of measured and calculated fluxes.

Plate 1. The downwelling SW (LW) flux difference between the binned and averaged values in 1-cm intervals of PWV and the monthly SW (LW) means during the clear-sky conditions at the ARM SCF. The NET flux is the sum of SW and LW fluxes in 1-cm intervals of PWV.

*Table captions*

TABLE 1. Accuracies of the archived downwelling and upwelling SW and LW fluxes at the ARM SCF from the Best Estimate Flux VAP.

TABLE 2. Seasonal and annual averages of cloud fraction at the ARM SCF.

TABLE 3. Seasonal and annual averages of SW/LW/NET clear-sky flux and CRF at the ARM SCF.

TABLE 4. Seasonal and annual averages of downwelling SW and LW fluxes at the ARM SCF.



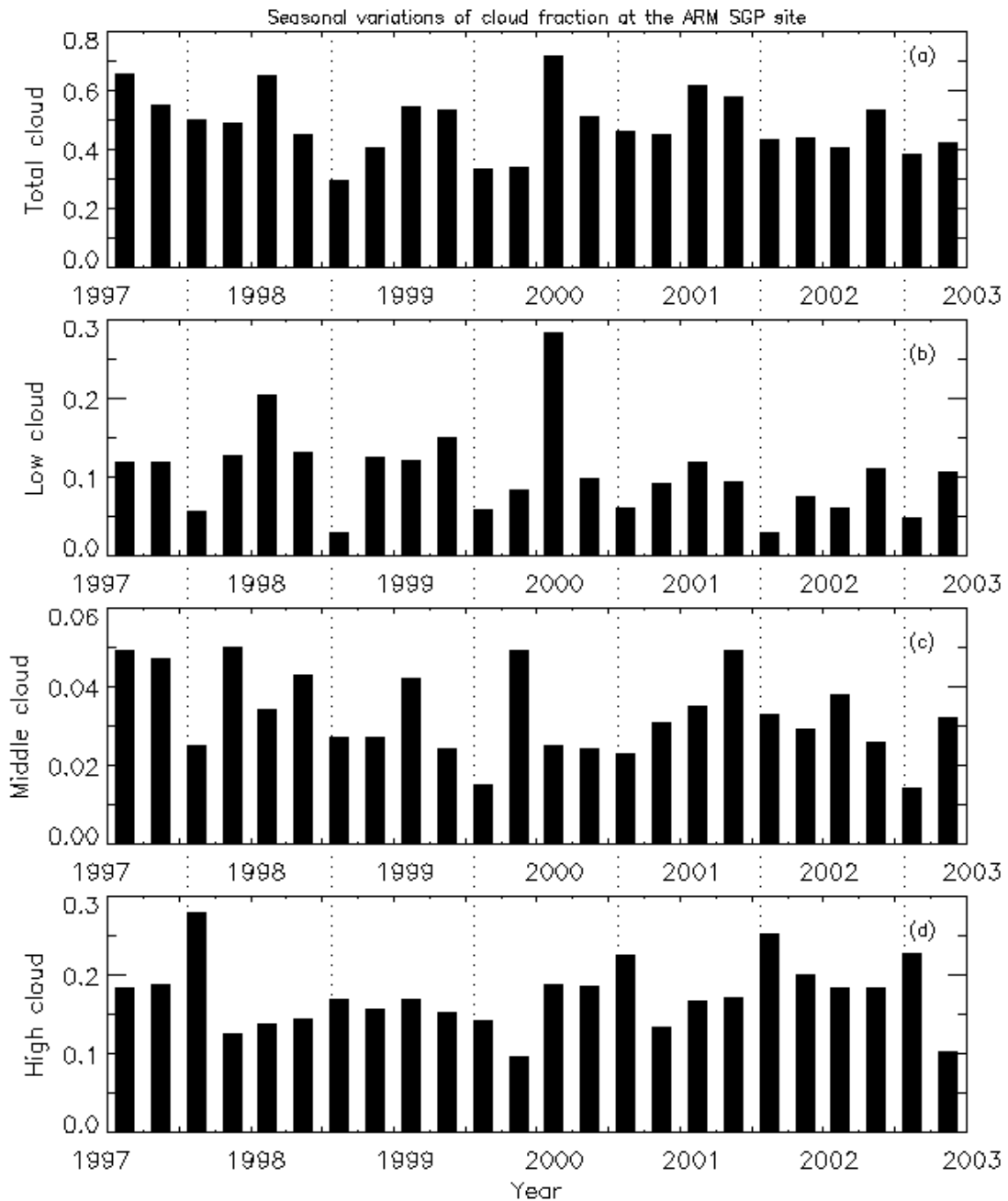


Fig. 1. The four seasons used in this study are DJF (winter), MAM (spring), JJA (summer), and SON (autumn). The total, and one-layer low ( $Z_b \leq 3$  km), middle ( $Z_b > 3$  km,  $Z_t \leq 6$  km), and high ( $Z_t > 6$  km) cloud fractions are defined as the lidar-radar measured cloud samples to the all-sky samples when all instruments of lidar/ceilometer, radar, downward and upward PSPs and PIRs were working simultaneously from January 1997 to December 2002 at the ARM SGP central facility (SCF). The dotted lines represent 6 summers during the 6-yr period.

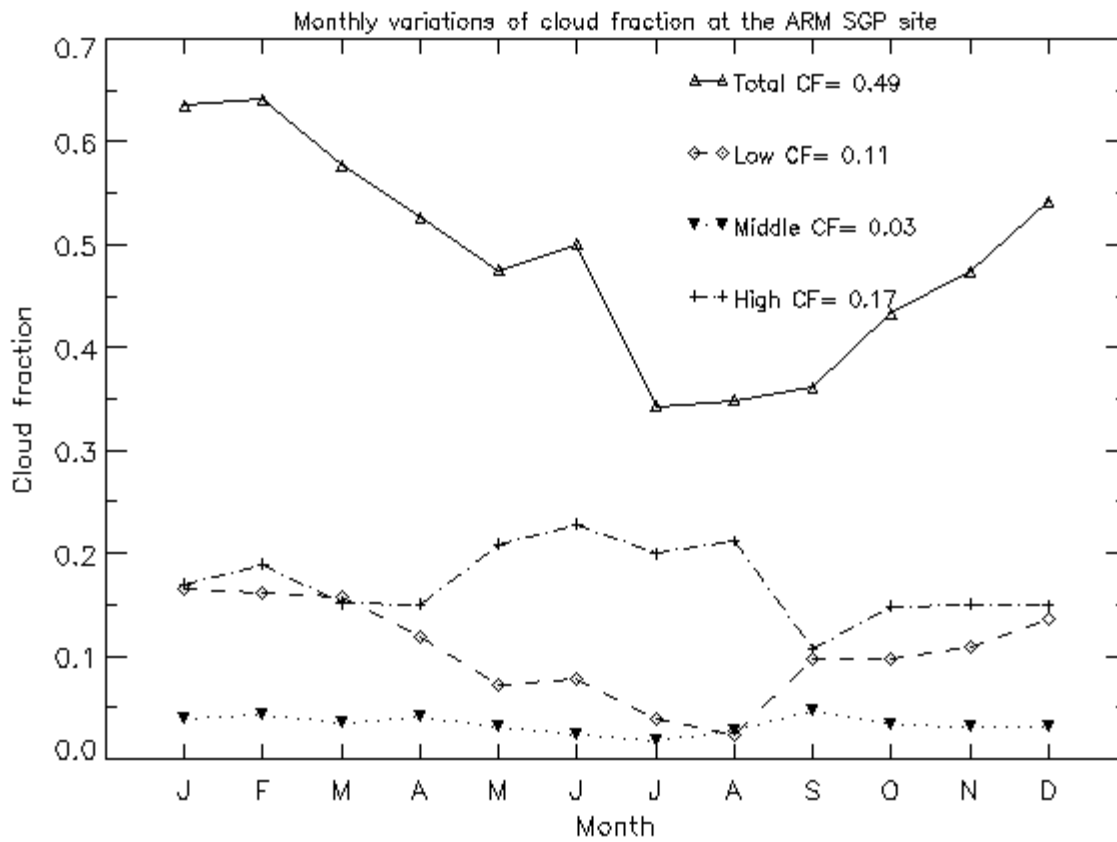


Fig. 2. Same as Figure 1, except for monthly means of cloud fractions derived from the 6-yr ARM SCF dataset.

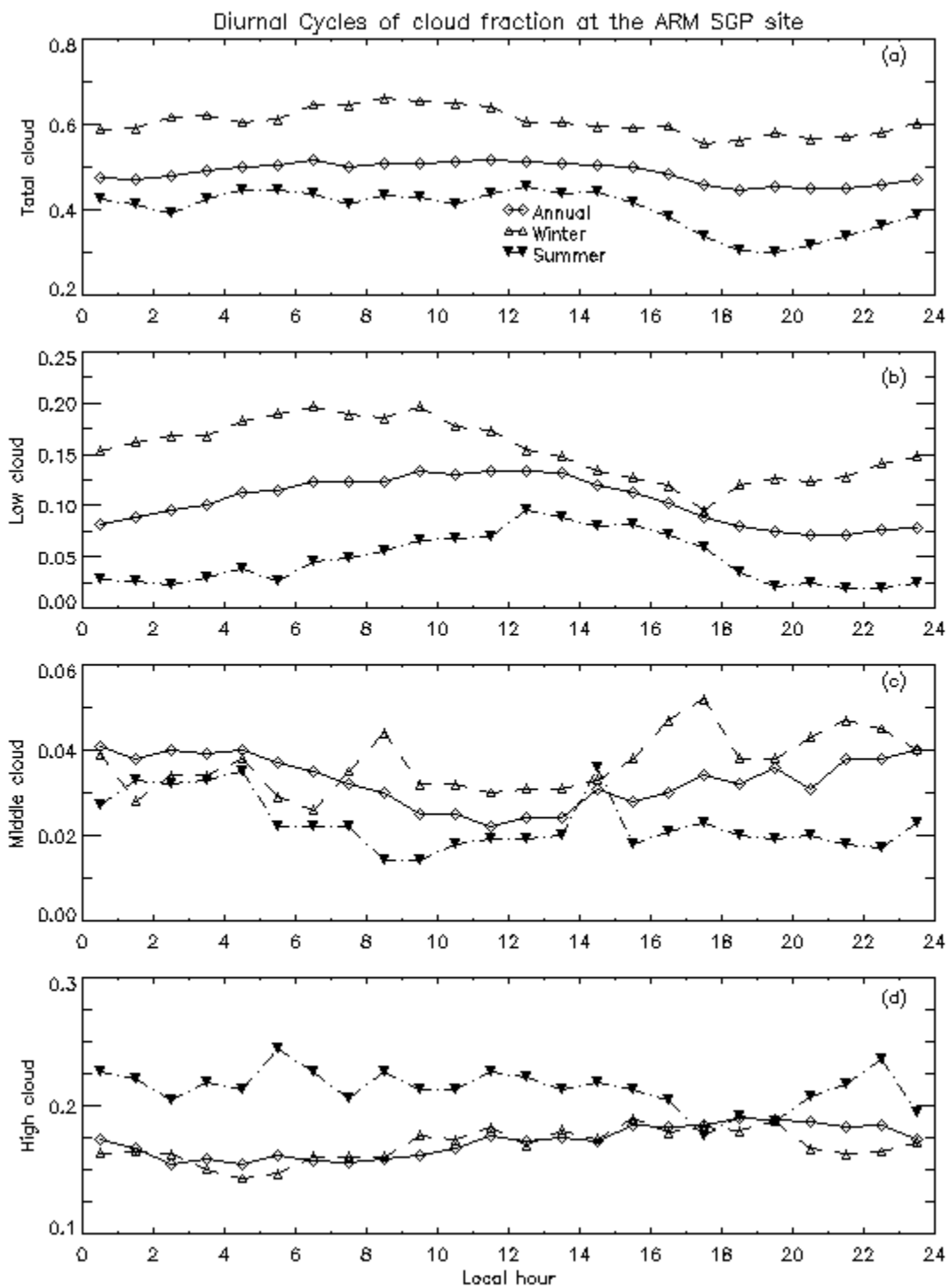


Fig. 3. Hourly averages of total, one-layer low, middle, and high cloud fractions for annual, winter, and summer seasons from the 6-yr dataset at the ARM SCF.

### Comparison of total cloud fraction at the ARM SGP Site

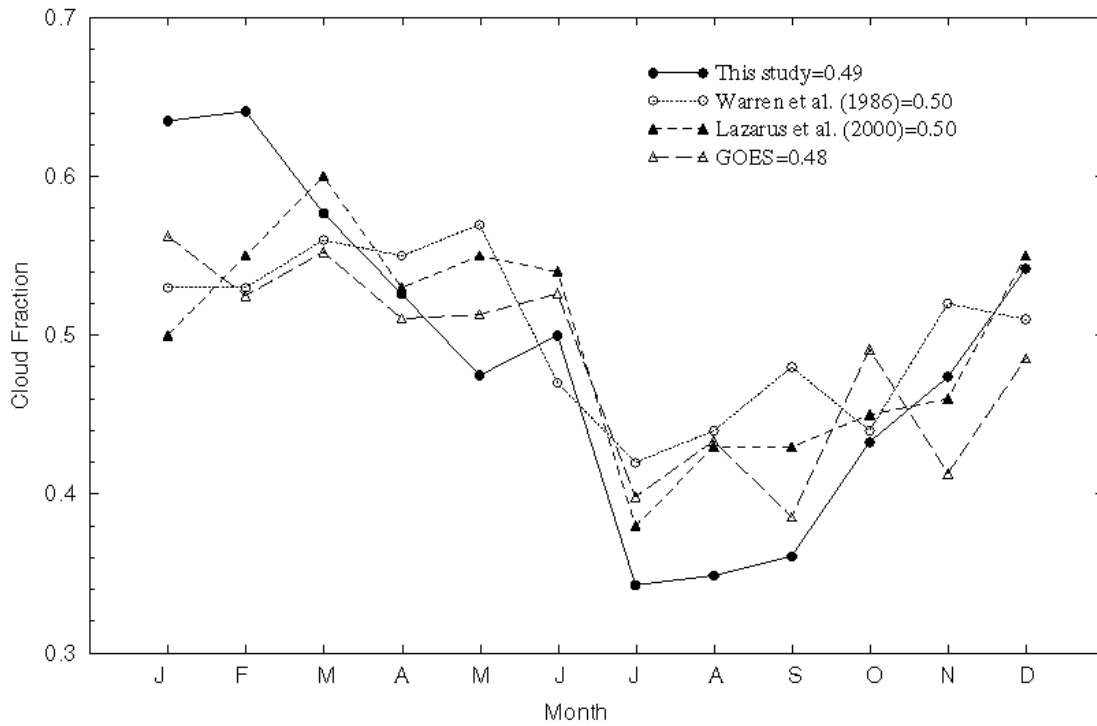


Fig. 4. The Warren et al. and Lazarus et al. studies were calculated from surface observations from January 1971 to December 1981 in a  $5^\circ$  region centered near the SCF, and from December 1981 to November 1991 at two stations (Oklahoma City, Oklahoma, and Wichita, Kansas) nearby the SCF, respectively. The GOES results are averaged over an area of  $0.3 \times 0.3$  degree centered on the SCF in the same time period as this study.

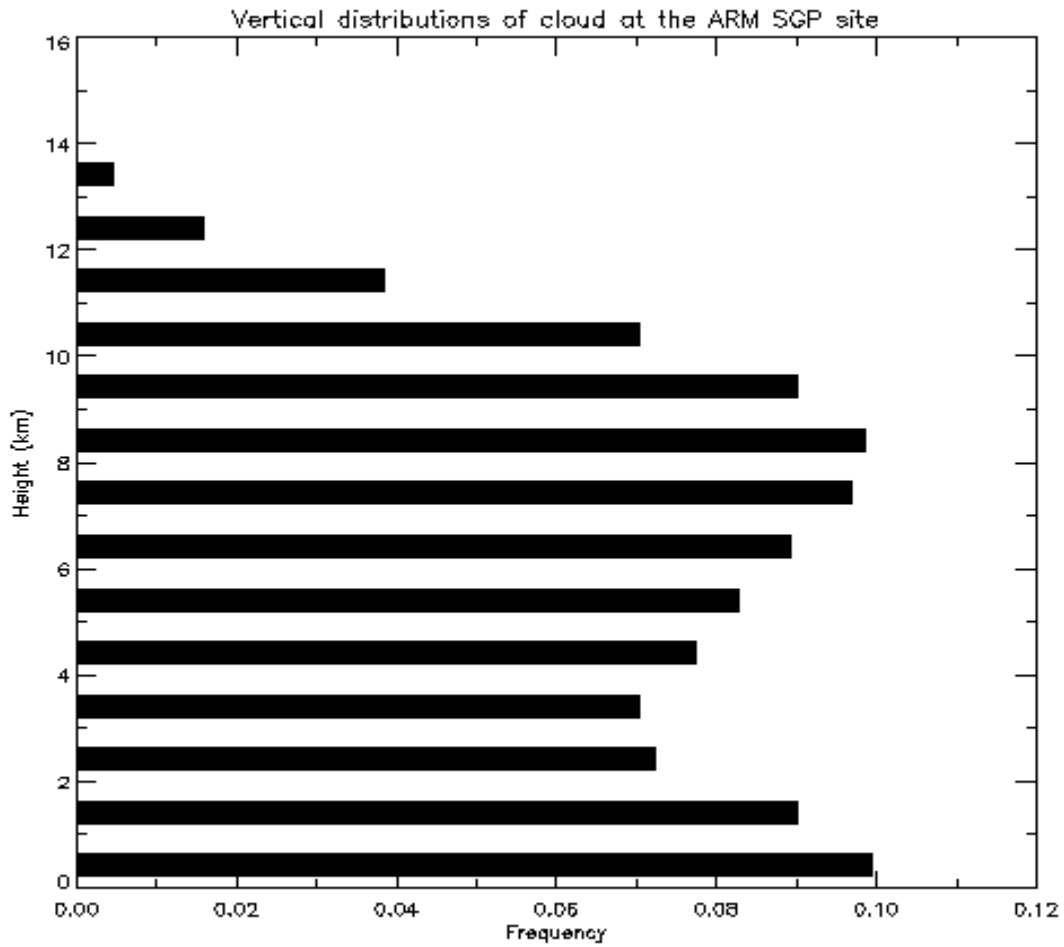


Fig. 5. Vertical distributions (1-km resolution) of total clouds at the ARM SCF during the 6-yr period.

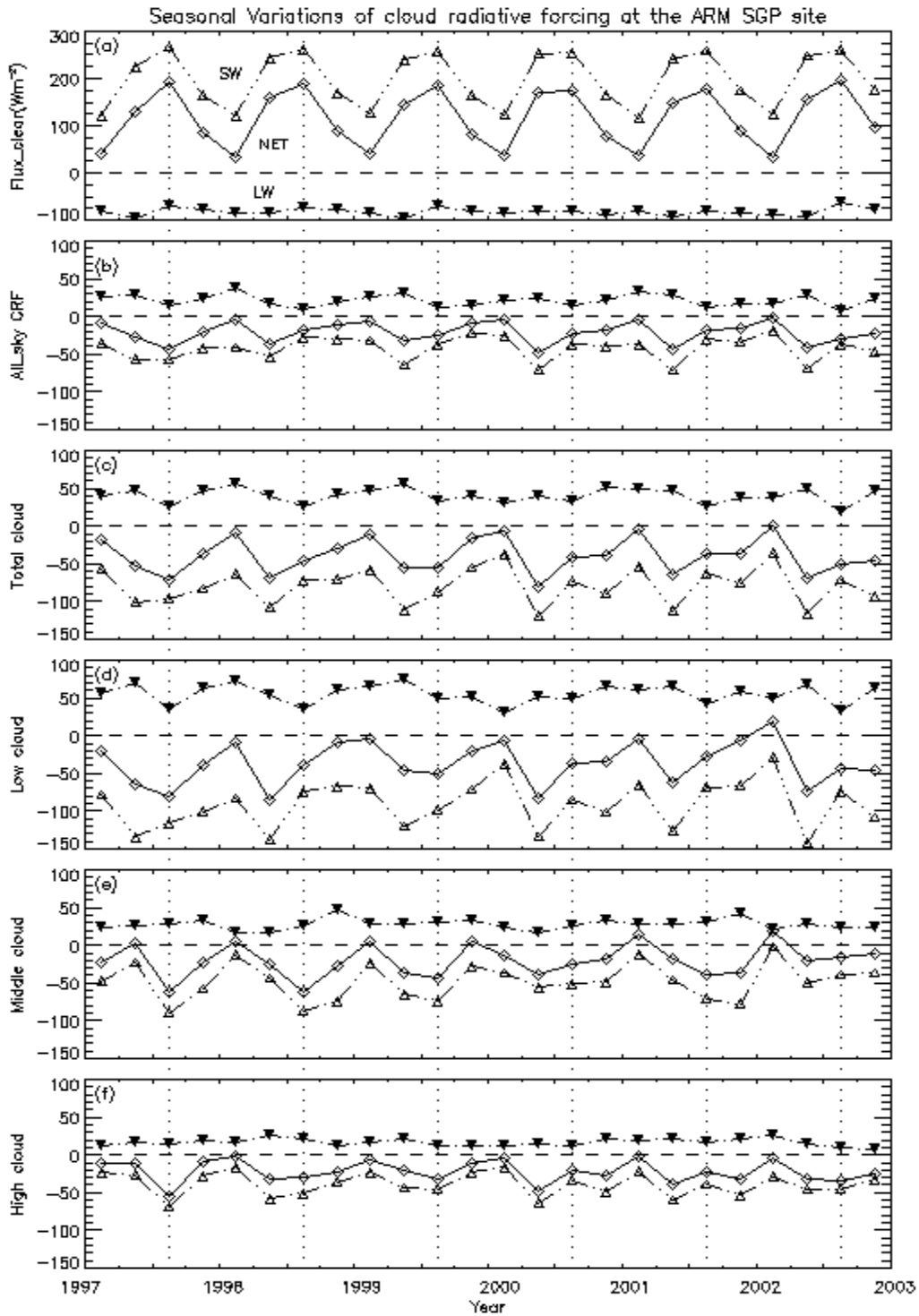


Fig. 6. Seasonal means of clear-sky net (down-up) LW and SW fluxes are calculated from the upward and downward PIR and PSP measurements when the sky was identified as cloudless by lidar-radar measurements. The seasonal LW (SW) CRF is the difference between cloudy and clear-sky LW (SW) means, and the seasonal net CRF is the sum of LW and SW CRFs (the values of net CRF are negative for cooling and positive for warming of the surface).

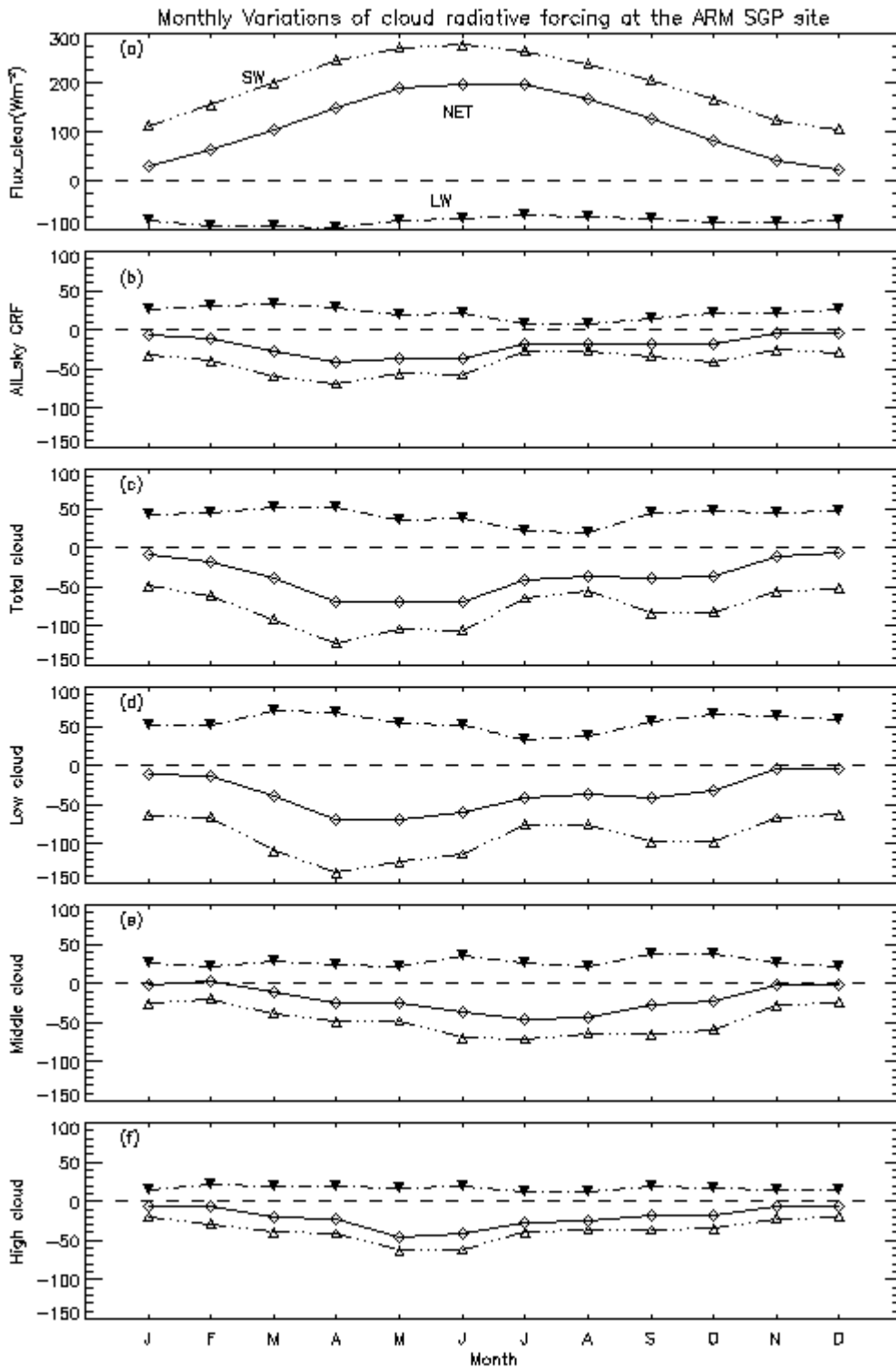


Fig. 7. Same as Figure 6, except for monthly means of clear-sky fluxes and cloud radiative forcings calculated from the 6-yr ARM SCF dataset.

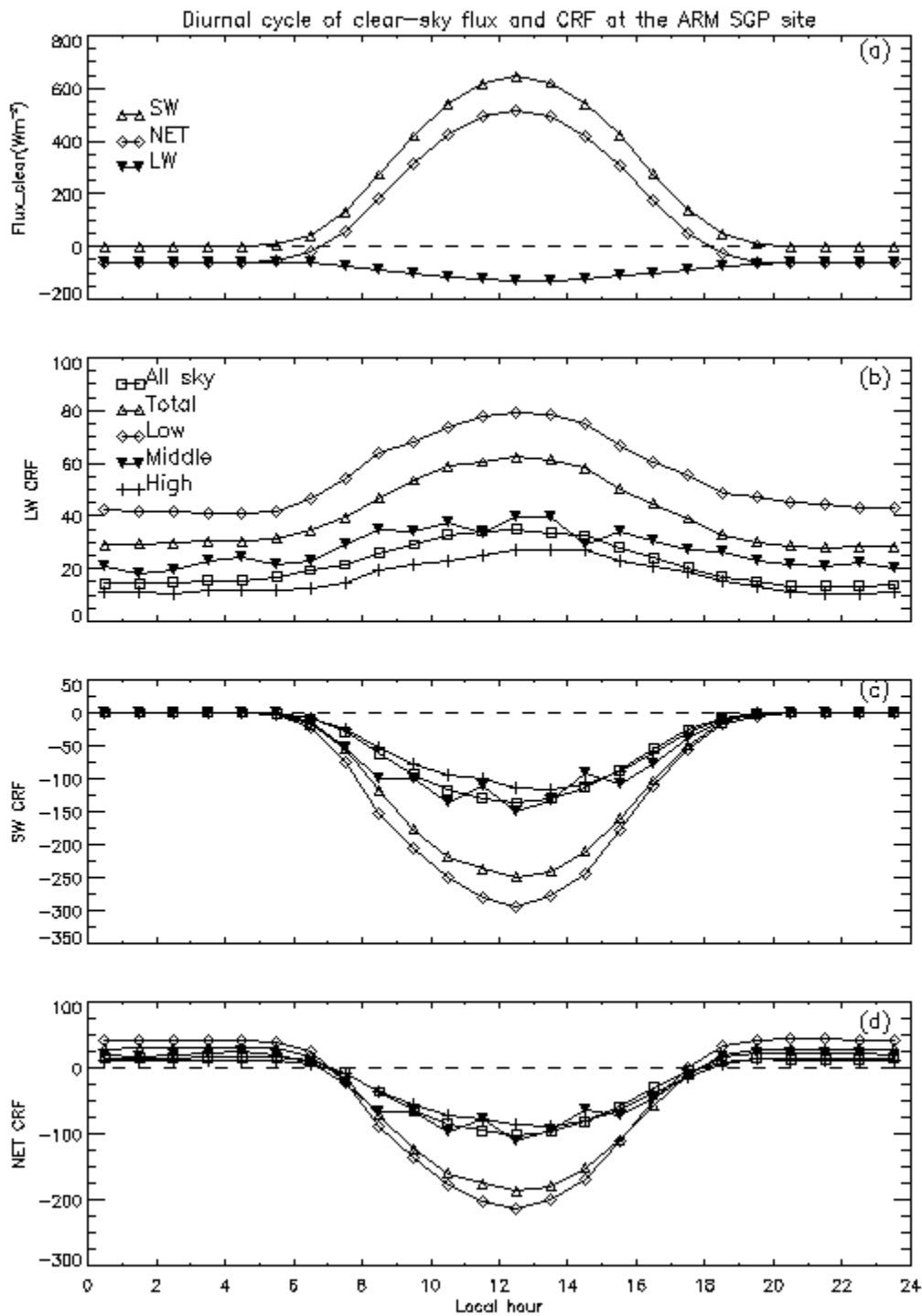


Fig. 8. Hourly averages of (a) clear-sky net SW/LW/NET fluxes, (b) LW, (c) SW, and (d) NET CRFs of all sky, total, low, middle, and high clouds during the 6-yr period at the ARM SCF.

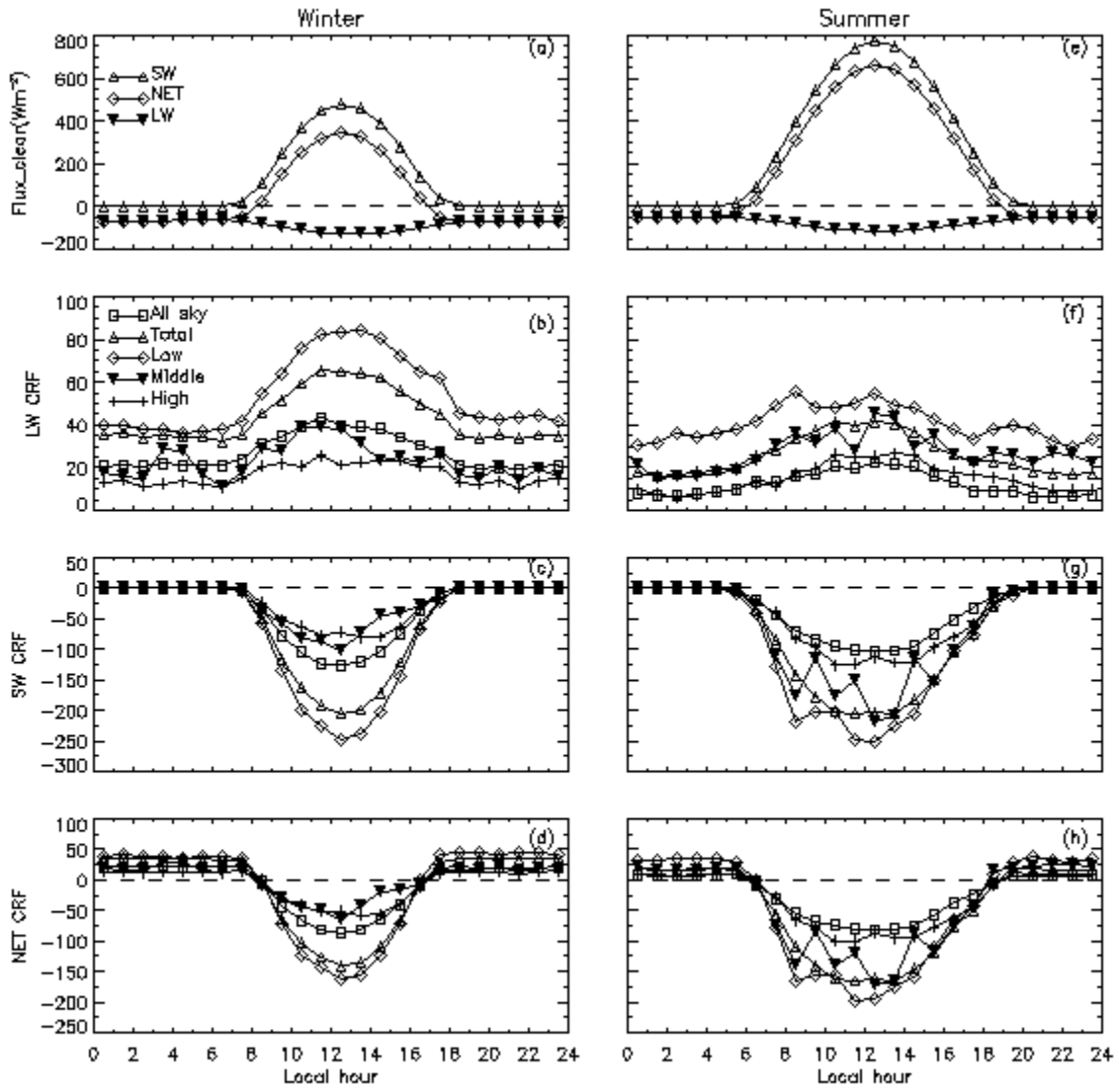


Fig. 9. Same as Figure 8, except for winter and summer seasons.

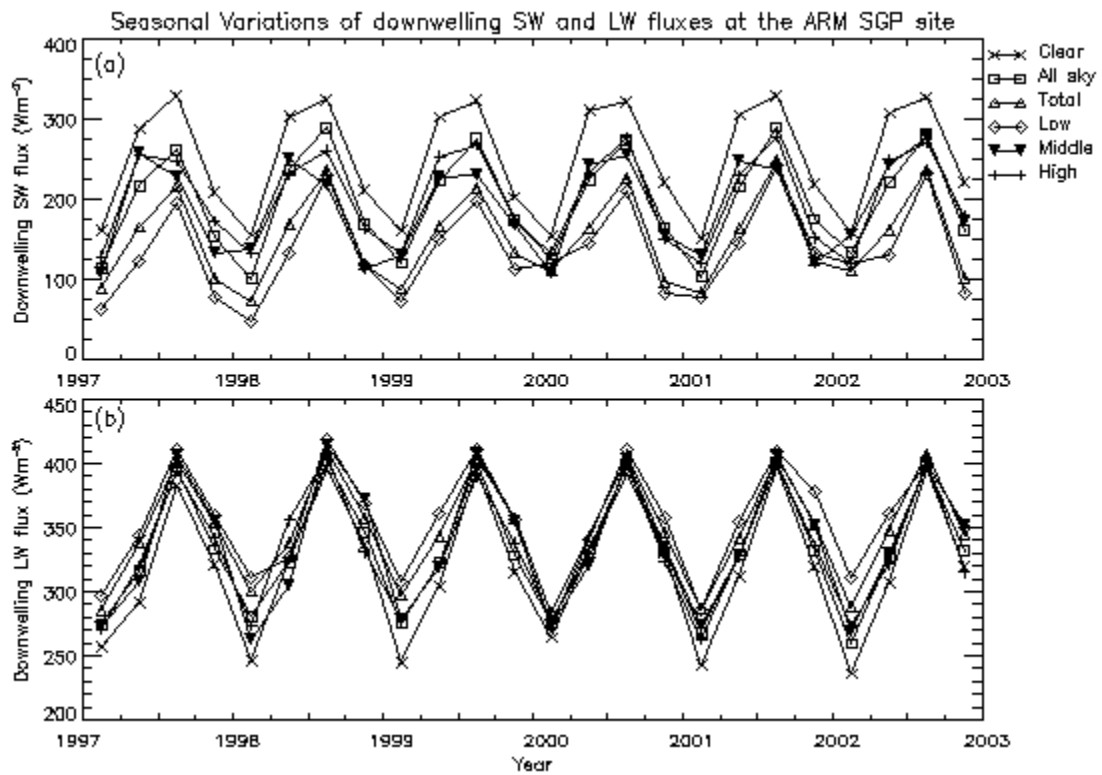


Fig. 10. Seasonal means of downwelling SW and LW fluxes measured by upward PSP and PIR, respectively, at the ARM SCF during the 6-yr period.

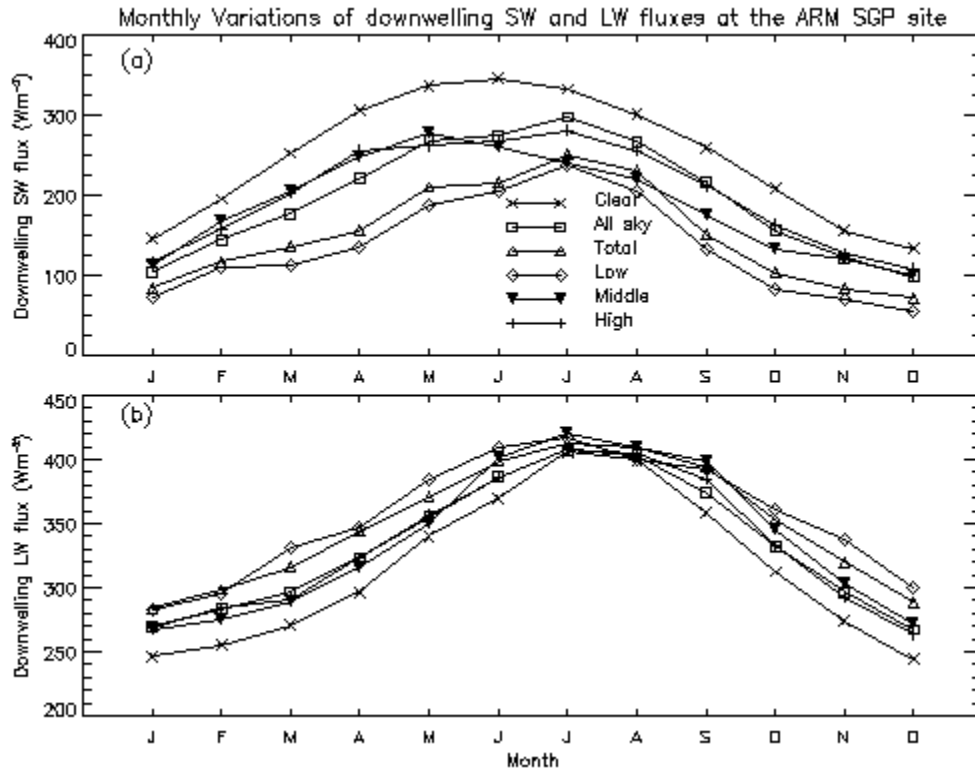


Fig. 11. Same as Figure 10, except for monthly means.

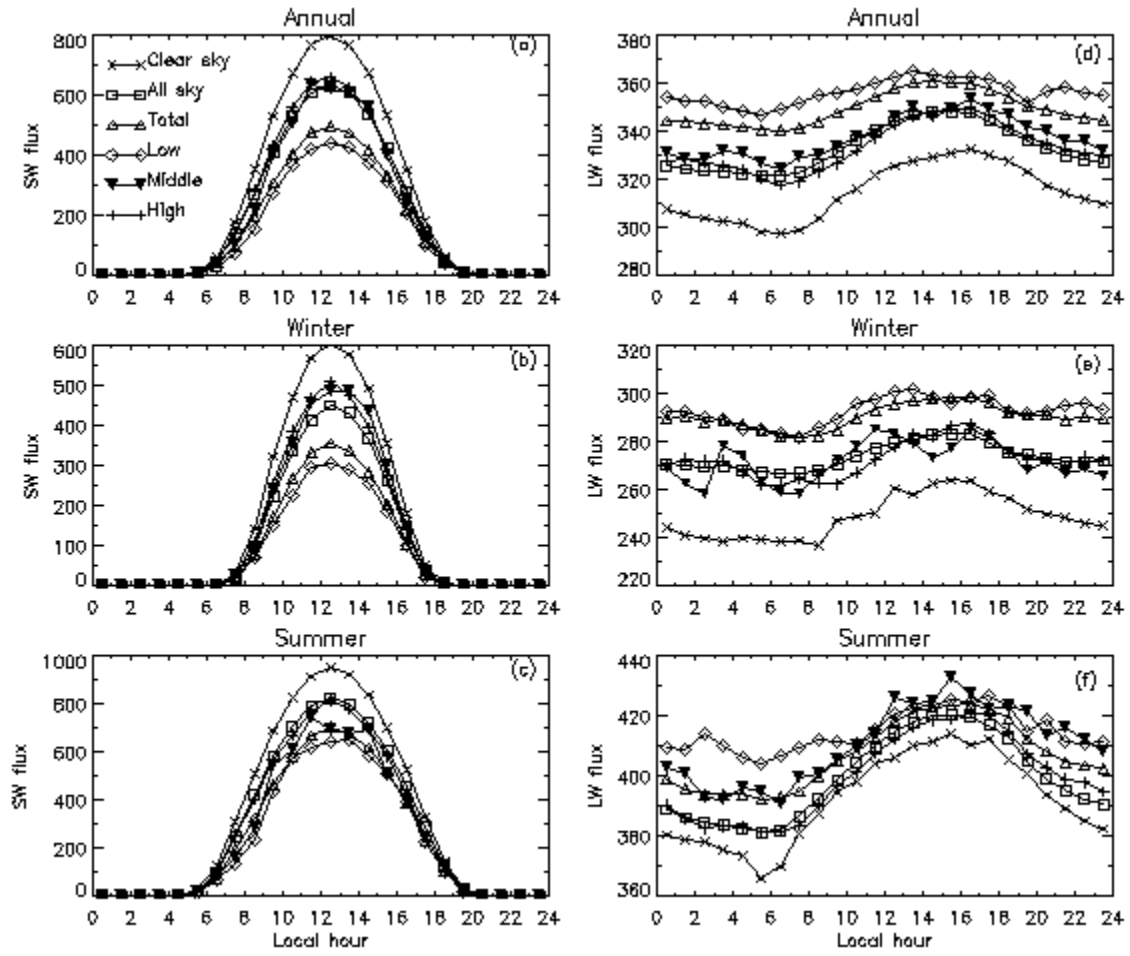


Fig. 12. Same as Figure 10, except for hourly means of annual, and winter and summer seasons.

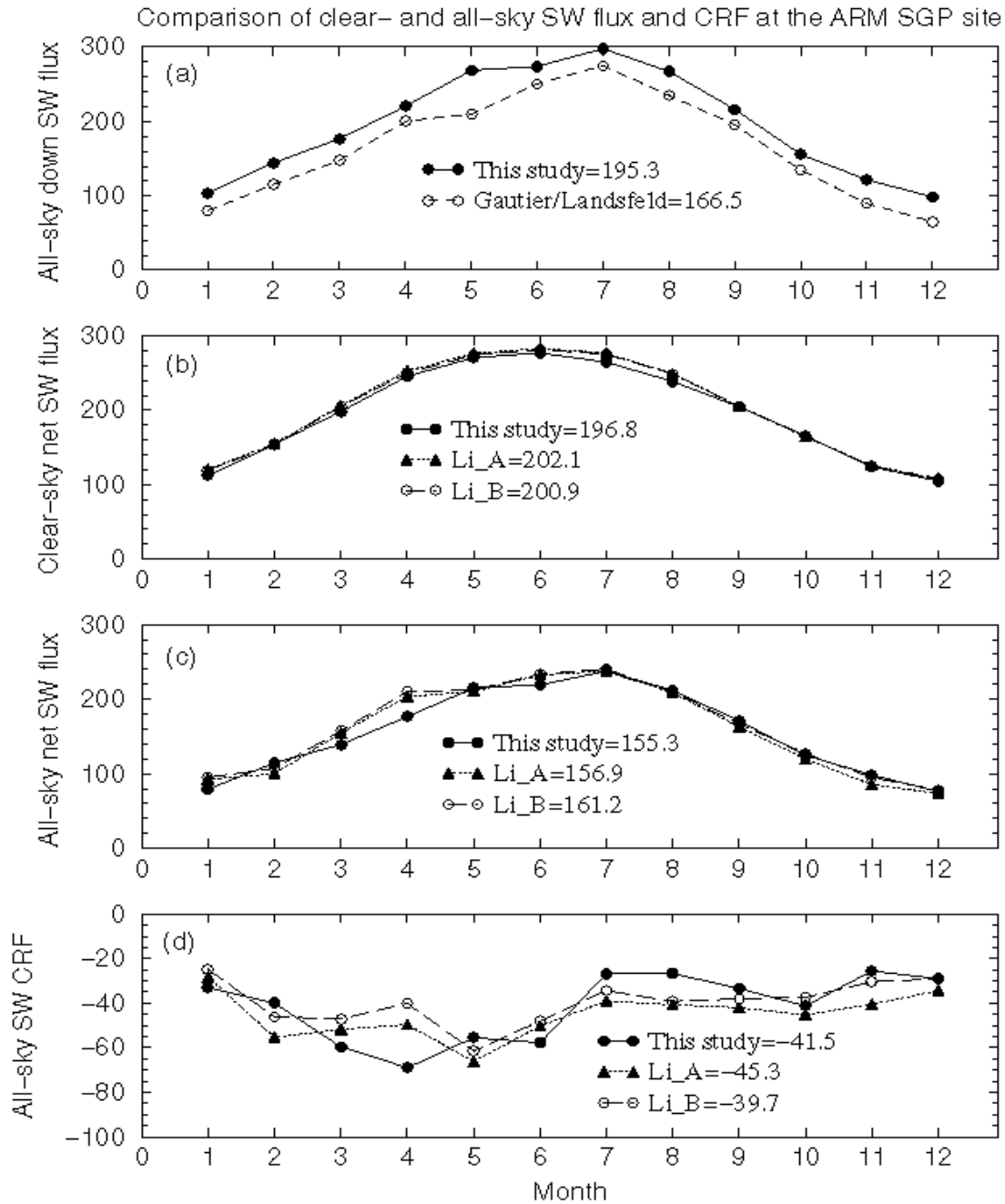


Fig. 13. The overall means are averaged from 12-month means. The monthly means of surface SW fluxes and CRFs in this study represent a point measurements at the SCF (36.6°N, 97.5°W) from January 1997 to December 2002, in Li and Leighton study represent a 2.5° X 2.5° spatial average including latitudes of 35 to 37.5°N, and longitudes of 95 to 97.5°W (Li\_B) and 97.5 to 100°W (Li\_A) from 5 years of ERBE data during the period of November 1984 to December 1989. The Gautier and Landsfeld results were averaged from 14 months of GOES-7 data between March 1993 and April 1994 over an area of 250-km X 250-km centered on the SCF.

Monthly variations of surface albedo and temperature, and atmospheric water vapor at the ARM SGP site

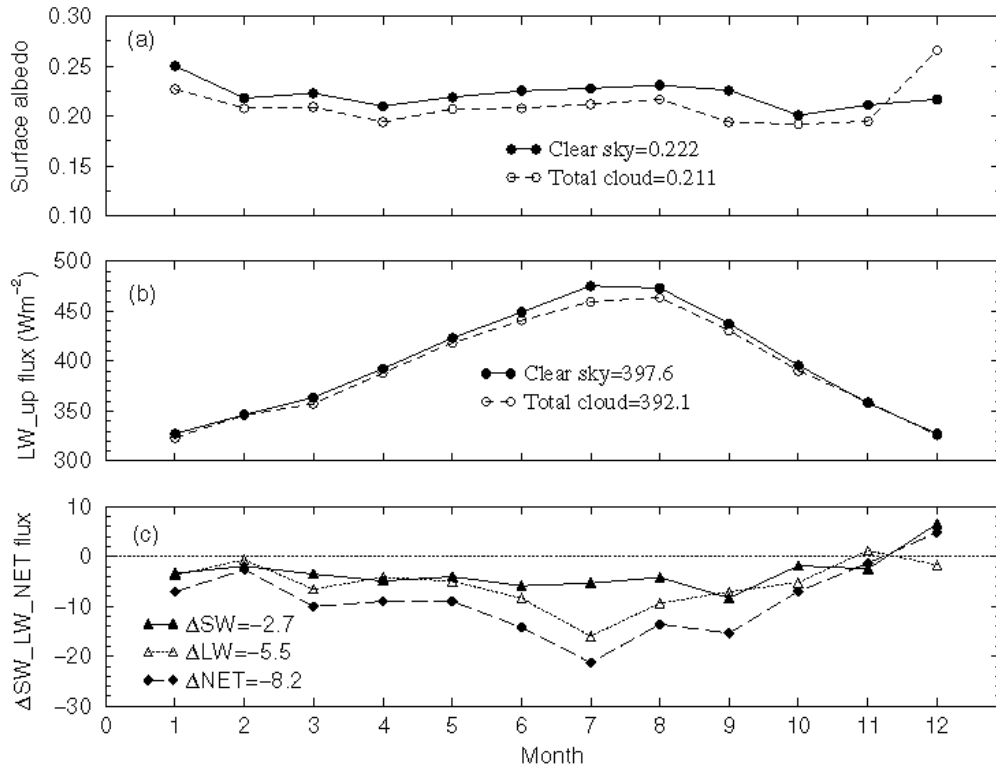


Fig. 14. Monthly means of clear-sky and total-cloud surface albedos (a) and upwelling LW fluxes (b). The monthly means of SW flux difference ( $\Delta SW$ ) are the product of downwelling clear-sky SW flux and surface albedo difference between cloudy and clear sky [ $SW_{clr}(R_{cld}-R_{clr})$ ],  $\Delta LW = LW_{cld} - LW_{clr}$ , and  $\Delta NET = \Delta SW + \Delta LW$ .

### Downwelling SW and LW vs. Water vapor at the ARM SGP site

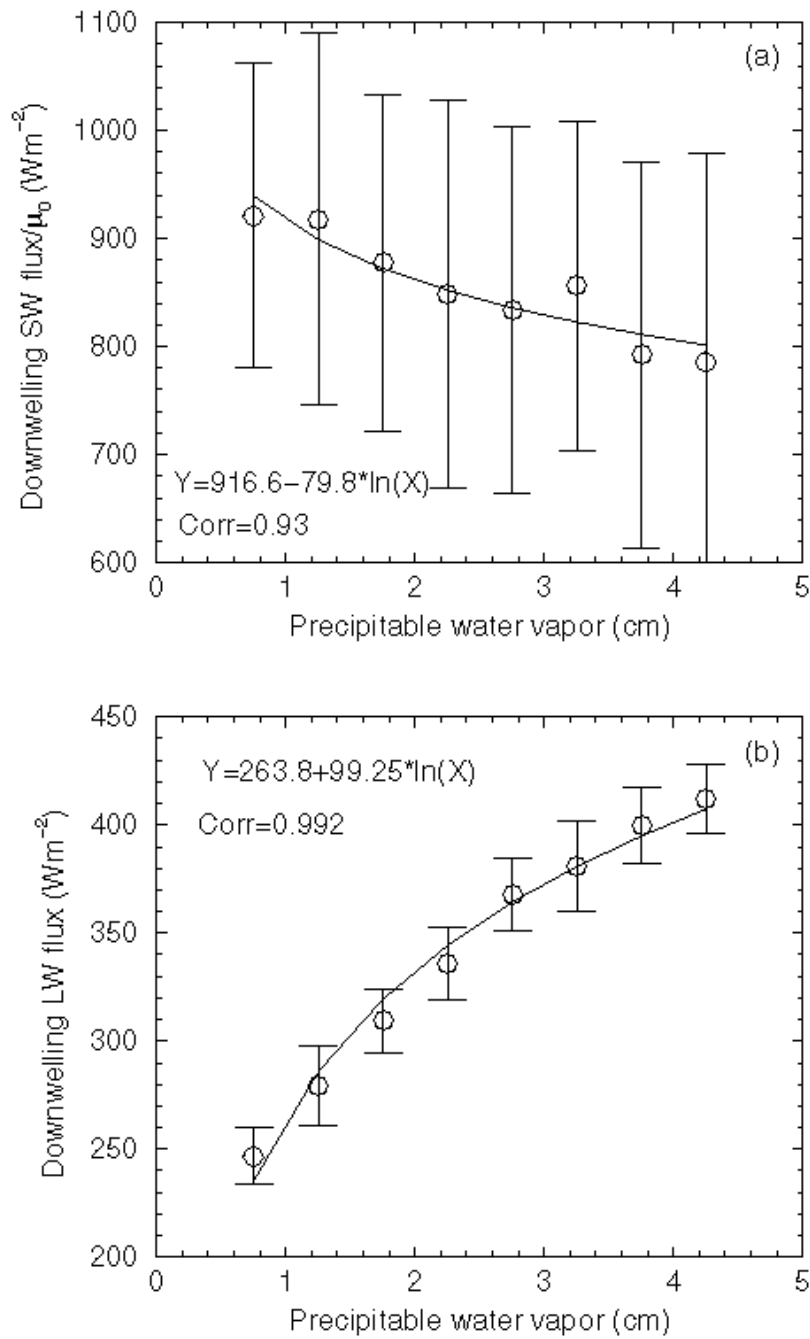


Fig. 15. Parameterizations of clear-sky downwelling SW/ $\mu_0$  and LW fluxes with precipitable water vapor (PWV) from a 0.5-cm interval (means and standard deviation) during the 6-yr period at the SCF.





### Water vapor correction for downwelling SW and LW fluxes

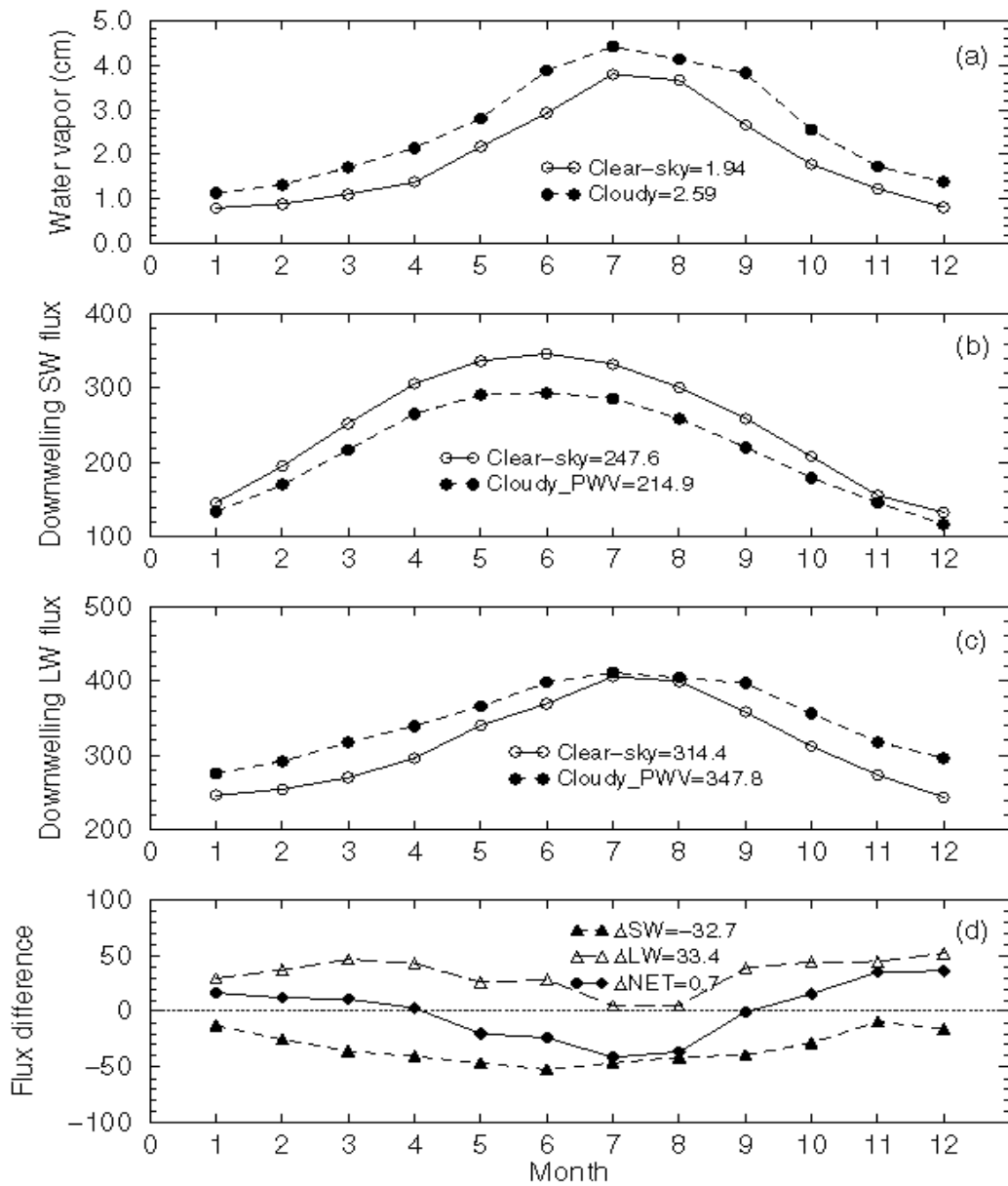


Fig. 16. (a) Monthly means of PWV during clear-sky and cloudy conditions, (b) the clear-sky downwelling measured SW/ $\mu_0$  flux and calculated SW/ $\mu_0$  flux using the new parameterization with cloudy PWV, (c) the clear-sky downwelling measured LW flux and calculated LW flux using the new parameterization with cloudy PWV, and (d) the difference of measured and calculated fluxes.



Downwelling SW & LW flux difference on Water Vapor

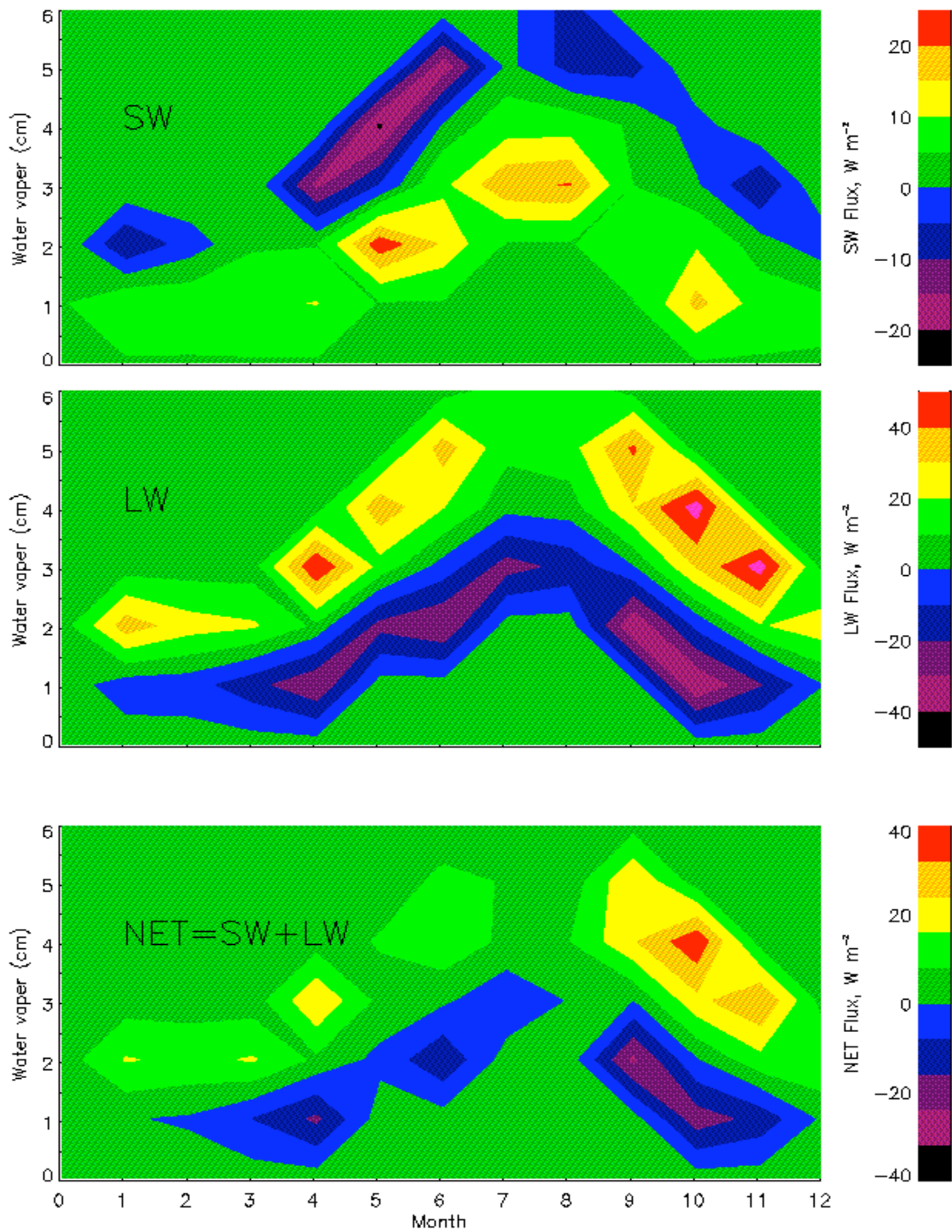


Plate 1. The downwelling SW (LW) flux difference between the binned and averaged values in 1-cm intervals of PWV and the monthly SW (LW) means during the clear-sky conditions at the ARM SCF. The NET flux is the sum of SW and LW fluxes in 1-cm intervals of PWV.

TABLE 1. Accuracies of the archived downwelling and upwelling SW and LW fluxes at the ARM SCF from the Best Estimate Flux VAP.

	Ideal accuracy ( $Wm^{-2}$ ) (Ohmura et al., 1998)	Best estimate ( $Wm^{-2}$ ) (Shi and Long, 2002)	Estimated accuracy of the BE Flux data ( $Wm^{-2}$ )
Diffuse SW	5.0	4.0 +/- 1.4	7.4
Direct Normal SW	2.0	6.3 +/- 3.3	9.8
Total SW	5.4	(Dir + Dif)	12.3
SW up	5.0	Typical: 11.1 +/- 2.8	10.6
LW down	10.0	3.1 +/- 0.4	10.6
LW up		Typical: 9.6 +/- 3.0	13.1

Note: The estimated accuracies of diffuse, direct, and total SW fluxes, as well as LW down are calculated as the  $SQRT([S\&L\_avg+dev]^2+[O]^2)$ , of LW up flux as the  $SQRT([2/3(S\&L\_avg+dev)]^2+[O\_LWdown]^2)$ , and of SW up flux as  $SQRT([2/3(S\&L\_avg+dev)]^2+[O]^2)$ .

TABLE 2. Seasonal and annual averages of cloud fraction at the ARM SCF

	Winter	Spring	Summer	Autumn	Annual
	D / W / L	D / W / L	D / W / L	D / W / L	D / W / L
$C_T, \%$	60 / 52 / 54	53 / 56 / 56	40 / 44 / 45	42 / 48 / 46	49 / 50 / 50
$C_L, \%$	16 / 25 / 27	12 / 23 / 28	5 / 7 / 16	10 / 22 / 21	11 / 19 / 23
$C_M, \%$	4 / 11 / 16	4 / 13 / 15	2 / 12 / 13	4 / 12 / 14	3 / 12 / 15
$C_H, \%$	17 / 35 / 26	17 / 34 / 28	21 / 25 / 24	14 / 27 / 20	17 / 30 / 25

D - This study  
W- Warren et al. (1986)  
L – Lazarus et al. (2000)

TABLE 3. Seasonal and annual averages of SW/LW/NET clear-sky flux and CRF at the ARM SCF

	Winter	Spring	Summer	Autumn	Annual
	SW / LW / NET				
Clear sky	123.8/ -85.3 /38.6	238.5/-90.8/147.8	260.1/-74.1/186.0	164.8/ -82.5/ 82.3	196.8/-83.1/113.7
All sky	-34.0/ 27.1 /-6.9	-61.3/ 26.4 /-34.9	-37.1/ 12.3 /-24.8	-33.4/ 19.8/ -13.6	-41.5/ 21.4/ -20.1
Total cloud	-54.1/ 43.7 /-10.4	-105.8/46.4/-59.4	-75.0/ 26.0/-49.0	-73.8/ 44.7/ -29.2	-77.2/ 40.2/ -37.0
Low cloud	-64.2/ 53.9 /-10.3	-123.0/63.7/-59.3	-87.6/ 40.7/ -46.9	-87.2/ 61.5 /-25.8	-90.5/ 55.0/-35.5
Mid cloud	-23.5/ 23.0 /-0.5	-45.2/ 24.5/-20.7	-68.2/ 26.8/-41.4	-50.9/ 34.4 /-16.5	-47.0/ 27.2/-19.8
High cloud	-22.9/ 16.7/ -6.3	-47.6/ 18.3 /-29.3	-46.2/ 15.1 /-31.1	-31.1/ 16.7 /-14.4	-37.0/ 16.7/ -20.3

TABLE 4. Seasonal and annual averages of downwelling SW and LW fluxes at the ARM SCF

	Winter		Spring		Summer		Autumn		Annual	
	SW	LW								
Clear Sky	158.1	248.6	298.3	302.5	326.3	391.9	207.6	314.7	247.6	314.4
All Sky	115.4	273.5	221.9	325.1	279.4	399.2	164.4	334.2	195.3	333.0
Total Cloud	90.8	290.3	167.2	343.7	232.2	406.7	112.7	355.7	150.7	349.1
Low Cloud	80.2	292.5	144.7	354.3	216.0	414.6	94.7	363.7	133.9	356.1
Mid Cloud	127.3	271.5	243.5	318.1	240.4	410.5	142.0	349.1	188.3	337.3
High cloud	128.1	272.5	240.0	323.8	268.2	399.5	167.6	336.9	201.0	333.2